REMARKS

This paper is submitted in response to the Office Action mailed May 5, 2004.

Claims 1-39 are pending. Claims 1-3, 7, 9-11, 13-15, 18-20, 28-30, and 36-39 have been amended, as discussed below. Support for the amendments can be found throughout the specification and claims as originally filed and there is no new matter added as a consequence of the new claims. Applicants reserve the right to continue prosecution of the cancelled subject matter in continuation applications.

Applicant would like to thank the Examiner for withdrawing the restriction requirement in response to the arguments presented in the response mailed September 29, 2004.

The Rejections under 35 U.S.C. § 112, ¶1 Should Be Withdrawn

Claims 1-17 and 35-39 are rejected under 35 U.S.C. § 112, first paragraph, because the specification while being enabling for producing a chimeric RNA in a cell *in vitro*, does not allegedly reasonably provide enablement for producing a chimeric RNA in a cell *in vivo* for the therapeutic treatment of conditions associated with papilloma virus pre-mRNA expression in a cell. The Examiner alleges that the specification does not enable any person skilled in the art to which it pertains or with which it is most nearly connected, to use the invention commensurate in scope with the claims. In particular, the Examiner alleges that the specification does not provide sufficient guidance such that the ordinary skilled artisan could use the teachings of the specification as filed as a guide to use the compounds of the present invention to treat conditions associated with defects in the coding region of the papilloma virus gene, in a method of gene therapy. Furthermore, the Examiner suggests that there are variety of factors associated with gene therapy which allegedly have not been overcome by routine

experimentation, such as the unpredictability of efficient delivery of gene therapy constructs. The Examiner alleges that the quantity of experimentation required to practice the claimed invention would encompass determining means such that all pre-trans-splicing molecules are all expressed in the same diseased cells at the same time and for a sufficient period of time such that the desired chimeric mRNA molecule is produced in a therapeutic amount to correct the defect in the diseased cells. The Examiner alleges that the specification is lacking specific guidelines, which leads the Examiner to conclude that undue experimentation is required, since the above-cited steps must be achieved before one is enabled to practice the claimed invention. Applicants respectfully traverse the rejection of claims 1-17 and 35-39.

Applicants submit that the specification provides support and guidance for one of skill in the art to make and use the full scope of the claimed invention without undue experimentation. The claimed invention must be enabled so that any person skilled in the art can make and use the invention without undue experimentation. *In re Wands*, 858 F2d. at 737, 8 USPQ2d at 1404 (Fed. Cir. 1988). Claims 1-17 and 35-39 relate to a cell that comprises PTMs capable of producing a chimeric RNA, where the PTMs contain a target binding domain specific to a viral or papilloma viral pre-mRNA, and methods of producing chimeric RNA using such PTMs. The specification discloses producing such chimeric RNA in 293 cells, transfected with a plasmid containing the entire HPV-16 early region (specification, Example 13, paras. 00260-00266, 00277). The specification also discloses a list of other cells that comprise HPV sequences, i.e. W12 (80263), which contain episomal HPV16 sequences (specification, para. 00276); and HPV-infected cancer cells (specification, paras. 00124, 00268), such as SiHa and CaSki cells, both of which contain integrated HPV16 sequences and are human cervical tumor cell lines (specification, para. 00276). The specification also discloses inhibition of the function

of papilloma virus RNA and the targeted killing of cancer cells by the expression of toxins, such as diptheria toxin sub unit A (specification, paras. 00124, 00268, 00273).

Applicants strongly disagree with the Examiner's contention that the specification fails to provide enablement for producing a chimeric RNA in a cell *in vivo* for the therapeutic treatment of conditions associated with papilloma virus pre-mRNA expression in a cell. Example 14 discloses a mouse model for papilloma infections using a xenograft technique (specification, paras. 00281). It discusses the animal model, how to create the model, what cells and viruses can be used, and clearly states that the disclosed animal model is used to test the *in vivo* efficacy of the anti-papillomavirus PTMs. Specifically, the specification discloses that various cells can be grafted onto the backs of nude mice, e.g. keratinocytes infected with human or bovine papilloma viruses grown on collagen and fibroblast rafts and human cervical carcinoma tissue or cell lines. Therefore, the specification clearly enables for *in vivo* application of the presently claimed nucleic acids and cells.

In fact, in accordance with the teachings of the specification, a recently published manuscript demonstrates *in vivo* application of PTMs targeted to HPV sequences to image expression of HPV E6 and E7 sequences in a live mouse (Bhaumik et al., "Molecular imaging of gene expression in living subjects by spliceosome-mediated RNA trans-splicing," Proc Nat Acad Sci, 2004, 101:8693-8698; attached as Exhibit 1). HPV sequences were inserted in a 3' position to part of the Renilla luciferase gene and transfected to create a stably transfected human breast cancer cell line. Twenty-four hours after the cells were injected into mice, PTMs containing a target binding domain to the HPV sequences and remaining 5' portion of the luciferase gene were injected into the tail vein of the mouse. The delivery of the PTMs (via liposomes) and

trans-splicing reaction *in vivo* was efficient enough to express luciferase to generate light that could be imaged through the living mouse.

Furthermore, the use of PTMs *in vivo* have been demonstrated in the correction of a Factor VIII deficiency (Chao et al., "Phenotype correction of hemophilia A mice by spliceosome-mediated RNA trans-splicing," Nature Medicine, 2003, 9:1-5; attached as Exhibit 2), and a CD-40 ligand deficiency (Tahara et al., "Trans-splicing repair of CD40 ligand deficiency results in naturally regulated correction of a mouse model of hyper-IgM X-linked immunodeficiency," Nature Medicine, 2004, 10:835-841; attached as Exhibit 3).

Applicants also disagree with the Examiner's conclusion that the specification is not enabling, based on the contention that a prerequisite to practicing the invention involves determining that "*all* pre-trans-splicing molecules are *all* expressed in the same diseased cells at the same time and for a sufficient period of time such that the desired chimeric mRNA molecule is produced in a therapeutic amount to correct the defect in the diseased cells." Contrary to the examiner's claim, the delivery of every PTM to every cell for expression of every PTM to promote trans-splicing is not required to confer a therapeutic benefit. Studies in various animal models show that cystic fibrosis, hemophilia A, and X-linked SCID can be corrected with low levels of trans-splicing. For example, expression of PTMs targeting endogenous mutant CFTR caused partial correction, *i.e.* approximately 22% of normal CFTR function, of the CFTR-mediated ion transport defect in a human bronchial xenograft model system (Liu et al., "Partial correction of endogenous DeltaF508 CFTR in human cystic fibrosis airway epithelia by spliceosome-mediated RNA trans-splicing," Nature Biotech. 20:47-52, attached as Exhibit 4). In fact, the correction of the CD40L deficiency through the administration of PTMs to CD40L knockout mice occurred with a trans-splicing efficiency as low as 1.2% (Tahara et al., p. 836,

col. 2, lines 31-33, Exhibit 3). In addition, a target pre-mRNA, spliced by a PTM, generates a chimeric RNA that can be translated multiple times. To promote translation of the chimeric RNA, the PTM may be designed to incorporate polyadenylation signals and protective groups to promote stability of the chimeric RNA product. Therefore, neither 100% delivery, 100% expression, nor 100% trans-splicing efficiency is required.

In contrast to RNAi or anti-sense strategies, which need to block all or nearly all disease causing mRNAs, the presently claimed compositions do not require each and every diseased transcript to be eliminated. For example, the expression of a single disease message to kill the cell, for example as in the use of diphtheria toxin subunit A, can be effective without having to target and eliminate each transcript. Therefore, applicants submit that the Examiner's requirement for elevated expression through a method of gene therapy is obviated. Applicants further submit that specification teaches that the PTM is administered in amounts effective to achieve a desired therapeutic effect (specification, para. 00148). Therefore, applicants assert that there is no undue experimentation required to practice the claimed invention and the full scope of claims 1-17 and 35-39 is enabled.

Claims 1-39 are also rejected under 35 U.S.C. §112, first paragraph, as failing to comply with the written description requirement. The Examiner alleges that the claims contain subject matter which was not described in such a way as to reasonably convey to one skilled in the art that the inventors, at the time the application was filed, had possession of the claimed invention. In particular, the Examiner alleges that the specification does not teach the skilled artisan how to predict the structures of the full scope of "target binding domains." The Examiner alleges that the skilled artisan would not be able to predict the actual structural description of the full scope of target binding domains that target binding of the nucleic acid molecules of the

invention to a papilloma virus pre-mRNA encompassed by the present claims. The Examiner alleges that the inventors do not have possession, because the specification does not provide an adequate description of the target binding domains, since the papilloma viruses are both species and cell-type specific.

Applicants submit that the specification provides adequate description of papilloma viruses in sufficient detail to have possession of the claimed invention. To satisfy the written description requirement, a patent specification must describe the claimed invention in sufficient detail that one skilled in the art can reasonably concluded that the inventor had possession of the claimed invention. See, e.g. *Vas-Cath, Inc. v. Mahurkar*, 935 F.2d at 1563, 19 USPQ2d at 1116. The specification discloses specific HPV16 regions, E6 and E7, used as the target sequences, since their gene products are expressed in cervical tumors. In addition, the specification discloses various papilloma viruses, e.g. human, bovine and other mammalian papilloma viruses. The sequences of bovine and mammalian papilloma viruses, e.g. equine, have been identified and are available through public databases, such as NCBI. Given the knowledge of the skilled artisan, the availability of various papilloma viral sequences, and the disclosure of specific examples of sequences from a human papilloma virus, applicants assert that one skilled in the art would reasonably conclude that the inventor had possession of the claimed invention. However, applicants have also amended claims 1-3, 7, 9-11, 13-15, 18-20, 28-30, and 36-39 to recite a *human* papilloma virus pre-mRNA. Support for the amendment can be found throughout the specification and claims as filed, and in particular, in para. 0125. Therefore, applicants submit that claims 1-39 satisfy the written description requirement.

For the foregoing reasons, Applicants respectfully request the withdrawal of the rejections under 35 U.S.C. § 112, first paragraph of claims 1-39.

Double Patenting Rejections

Claims 1-39 are rejected under the judicially created doctrine of obviousness-type double patenting as being unpatentable over claims 1-39 of U.S. Patent No. 6,013,487 in view of Hendricks et al. (U.S. Patent No. 5, 580,970A).

Applicants will submit a terminal disclaimer, if appropriate, once Applicants have successfully overcome the remaining outstanding rejections and the Examiner has indicated allowance of claims.

Applicants further submit that the claims of the present invention are not anticipated by or obvious over the claims of Hendricks et al. Hendricks does not claim the cells, nucleic acids or methods of the present invention and cannot be used in combination with another reference in a double patenting rejection.

CONCLUSION

In view of the foregoing, we respectfully submit that all pending claims are allowable and that the application is otherwise in condition for allowance. Applicants respectfully request the issuance of a Notice of Allowance.

Applicants request a three month extension of time and encloses herewith the requisite fee as set forth in 37 C.F.R. § 1.17(a)(3). Applicant does not believe that any additional fee is required in connection with the submission of this document. However, should any fee be required, or if any overpayment has been made, the Commissioner is hereby authorized to charge any fees, or credit any overpayments made, to Deposit Account 02-4377. A duplicate copy of this sheet is enclosed.

Respectfully submitted,

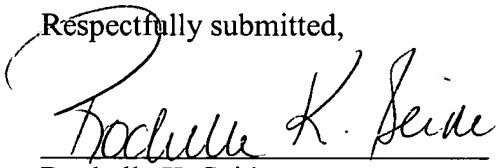

Rochelle K. Seide
Patent Office Reg. No. 32,300
Attorney for Applicants

Dana Lau
Patent Office Reg. No. 55,361
Agent for Applicants

BAKER BOTTS L.L.P.
30 Rockefeller Plaza
New York, New York 10112-4498
(212) 408-2500

Form PTO-1449 U.S. Department of Commerce REV. 2-82) Patent and Trademark Office	Atty. Docket No. A33778 (067252.0106)	Serial No. 10/012,269
INFORMATION DISCLOSURE STATEMENT BY APPLICANT	Applicant Smith *et al.*	
(Use several sheets if necessary)	Filing Date 11/06/2001	Group 1645
	Examiner Minnifield, Nita	

U.S. PATENT DOCUMENTS

*Exam. Initial.	No.		Document No.	Date	Name	Class	Subclass	Filing Date if Approximate.

FOREIGN PATENT DOCUMENTS

Exam Initial	No.		Document No.	Date	Country	Class	Subclass	Translation Yes No
	1.		WO 99/20306	29 Apr. 1999	Int'l WIPO	A61K	39/08	
	2.		WO 98/07864	26 Feb. 1998	Int'l WIPO	C12N	15/31	
	4.		WO 95/327380	7 December 1995	Int'l WIPO	A61K	47/48	

Exam Initial	No.		**OTHER DOCUMENTS (including Author, Title, Date, Pertinent Pages, Etc.)**
	3.		Aguado F. et al., 1997, "Regulated secretion is impaired in AtT-20 endocrine cells stably transfected with botulinum neurotoxin type a light chain" J. Biological Chemistry, vol. 272, no. 41, 10 October 1997 pages 26005-26008.

NY02:445124.2

Examiner Date Considered

* Examiner: Initial citation considered, whether or not citation is in conformance with MPEP 609; Draw line through citation if not in conformance and not considered. Include copy of this form with next communication to applicant.

Molecular imaging of gene expression in living subjects by spliceosome-mediated RNA trans-splicing

S. Bhaumik*, Z. Walls*, M. Puttaraju†, L. G. Mitchell†, and S. S. Gambhir*‡

*Department of Radiology and Bio-X Program, Stanford University, James H. Clark Center E150, 318 Campus Drive, Stanford, CA 94305-5427; and †Intronn Inc., 910 Clopper Road, South Building, Suite 210, Gaithersburg, MD 20878

Communicated by Michael E. Phelps, University of California School of Medicine, Los Angeles, CA, April 19, 2004 (received for review February 2, 2004)

Spliceosome-mediated RNA trans-splicing (SMaRT) provides an effective means to reprogram mRNAs and the proteins they encode. SMaRT technology has a broad range of applications, including RNA repair and molecular imaging, each governed by the nature of the sequences delivered by the pre-trans-splicing molecule. Here, we show the ability of SMaRT to optically image the expression of an exogenous gene at the level of pre-mRNA splicing in cells and living animals. Because of the modular design of pre-trans-splicing molecules, there is great potential to employ SMaRT to image the expression of any arbitrary gene of interest in living subjects. In this report, we describe a model system that demonstrates the feasibility of imaging gene expression by trans-splicing in small animals. This represents a previously undescribed approach to molecular imaging of mRNA levels in living subjects.

mRNA repair | gene correction | reporter

In the postgenomic era, a great impetus has been generated toward designing therapeutic and diagnostic agents that are able to capitalize on the wealth of genetic information now available. Although proteins are the ultimate effectors of genetic programming, there are several preceding steps in the cascade of gene expression where interventions for therapy or diagnosis are possible. Because of the complex tertiary folding and singular structure of each individual protein, it is unfeasible (at present) to design molecules specific for an arbitrary protein based on sequence alone. However, given that the principles behind targeting arbitrary nucleic acid sequences have been well established (1) and our profound knowledge of the human genomic sequence, it is practicable to design molecules that interact with specific genes at the nucleotide level. By exploiting the Watson–Crick base-pairing nature of nucleic acids, researchers have been able to design sequence-specific molecules for purposes ranging from *in vivo* antisense therapeutics to *in vitro* detection (2, 3).

The concept of therapeutic intervention at the level of nucleic acids has been advanced recently by spliceosome-mediated RNA trans-splicing (SMaRT) (4, 5). SMaRT has effectively repaired disease-causing mutant genes at the level of RNA splicing for several disorders including hemophilia and cystic fibrosis (6, 7). The principle behind SMaRT is centered on the use of engineered pre-trans-splicing molecules (PTMs), which can replace the mutated portion of a disease-causing gene with the wild-type sequence. SMaRT can also be used to regulate the trans-splicing and expression of almost any desired gene sequence, such as those encoding reporter or toxic molecules (4, 8). Embedded within each PTM are active splicing elements that are recognized by the cell's splicing machinery. These promote the formation of spliceosome complexes that trans-splice the PTM encoded exon(s) into the target transcript rather than allowing cis-splicing within the target pre-mRNA to occur. The specificity of the trans-splicing reaction is conferred primarily by the binding domain of the PTM, which is designed to be complementary to intronic sequences in the target of interest (8).

Building on the previous successes with therapeutic applications of SMaRT (6, 7), we decided to apply this platform technology to the field of molecular imaging by reprogramming expressed pre-mRNAs to encode reporter molecules that are used for imaging purposes. The rapidly emerging field of molecular imaging has concerned itself with designing strategies for noninvasively investigating molecular events on a global scale in living animals (9). To do so, various modalities are used, including cooled charge-coupled device (CCD) cameras for optical imaging, single-photon emission computed tomography (SPECT), and positron emission tomography (PET) for radionuclide imaging and MRI (9). Given the rapid production and highly modular nature of designing antisense oligonucleotide probes for nucleic acid targets, a key goal for this field is to develop a system for imaging any arbitrary nucleic acid sequence *in vivo*. Accomplishing this objective would allow investigators to target and image the expression of any gene of interest.

Our strategy for imaging mRNA with SMaRT technology has several advantages over more classical methods, such as radiolabeled antisense oligonucleotides (RASONs), but retains the specificity for targeting endogenous nucleic acids. Fig. 1 highlights the attributes of SMaRT for imaging endogenous mRNA. As a genetically encoded imaging system, SMaRT possesses the advantage of signal amplification at multiple steps (an attribute that antisense oligonucleotides do not have). Multiple hybrid proteins are translated for each composite mRNA produced, and if the protein encoded is an enzyme, each of these can convert many substrate molecules, resulting in multiple signals generated for each recognition event.

To demonstrate the potential of SMaRT for imaging the expression of an mRNA, we constructed a target gene consisting of a portion encoding for the *Renilla* luciferase bioluminescent protein coupled to intronic and exonic sequences from the human papillomavirus type 16 (HPV-16). *Renilla* luciferase was chosen because it has proven to be a very sensitive bioluminescent reporter (10). Sequences from HPV-16 were used because of their clinical relevancy and sequence familiarity. Expressed alone, the *Renilla* protein fragment does not possess any bioluminescent activity. To generate luciferase, we engineered a PTM containing the remaining portion of *Renilla* luciferase as a "3′ exon" and a binding domain specific for HPV-16. When the PTM trans-splices specifically into the target pre-mRNA, full-length *Renilla* luciferase mRNA and functional protein are produced, generating a bioluminescent signal. In this report, we show that SMaRT technology can create enzymatic activity and that the resultant signal can be detected both in cell culture and living animals.

Methods

Recombinant Pre-mRNA Target and Trans-Splicing PTM Constructs. To investigate the potential use of SMaRT for molecular imaging of gene expression, a model system was designed by using the synthetic *Renilla* luciferase (hRLuc) bioluminescent reporter

Abbreviations: SMaRT, spliceosome-mediated RNA trans-splicing; PTM, pre-trans-splicing molecules; RASON, radiolabeled antisense oligonucleotide; HPV, human papillomavirus; N2a, neuro-2a; ROI, region of interest; sr, steridian.

‡To whom correspondence should be addressed. E-mail: sgambhir@stanford.edu.

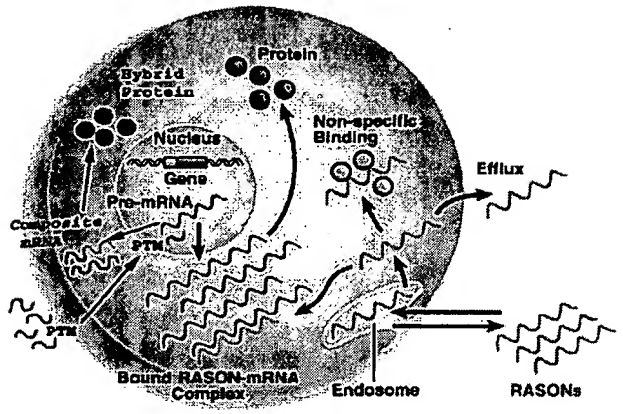

Fig. 1. Advantages of SMaRT over RASONs. RASONs are designed to hybridize to target mRNA to produce imaging signal. The SMaRT strategy uses trans-splicing of target mRNA to lead to hybrid proteins that are capable of being imaged. RASONs are limited in their use for *in vivo* imaging by several problems including nonspecific binding to proteins, a lack of efflux when no target mRNA encountered, and a limited amount of signal produced for each detection event. SMaRT has the advantages in delivery of a genetically encoded system as well as several stages of signal amplification that make it a more promising approach to *in vivo* imaging of mRNA.

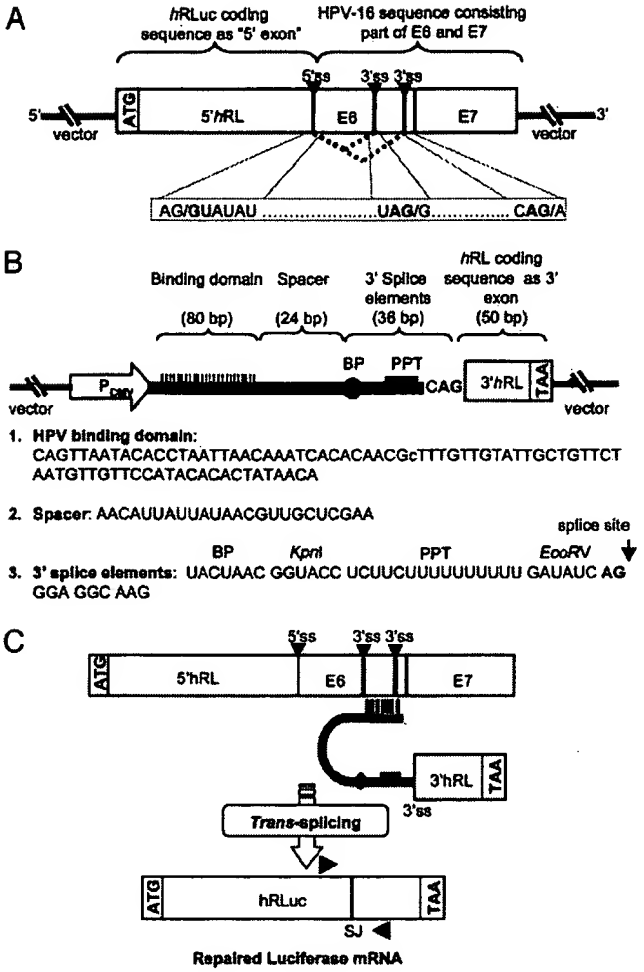

Fig. 2. Schematic diagrams of the PTM and pre-mRNA target used for imaging gene expression. (*A*) The pre-mRNA target, LucHPVT3, contains the N-terminal portion of hRLuc coding sequence coupled to exonic and intronic sequences of the HPV-16 E6 and E7 oncoproteins. Dotted lines indicate cis-splicing of the target. (*B*) LucPTM37 codes for the trans-splicing components (binding domain, spacer, and 3′ splice elements) as well as the C terminus portion of the hRLuc coding sequence. (*C*) Schematic representation of SMaRT reaction. Arrows indicate target (forward) and PTM (reverse) primers used for measuring specific trans-splicing. BP, branchpoint; PPT, polypyrimidine tract; ss, splice site; SJ, splice junction.

gene. This prototype system is predicated on data that show that the hRLuc gene can be split into separate halves, which, if expressed individually, retain little to no bioluminescent activity in the presence of coelenterazine substrate (11). Thus, two plasmid constructs were generated, one that codes for the target pre-mRNA and contains the N terminus portion of the hRLuc gene as well as intronic and exonic sequences from the E6 and E7 oncoproteins of the HPV-16 (Fig. 2*A*). The other construct codes for the HPV target-specific PTM and contains the C terminus portion of the hRLuc gene as well as the components necessary to produce trans-splicing (Fig. 2*B*). These trans-splicing elements include a binding domain (BD) complementary to the target, a short spacer, and 3′ splice elements (branch point, polypyrimidine tract, and acceptor AG). The BD localizes the PTM and its active splice site to the vicinity of the target pre-mRNA. This interaction facilitates the specific trans-splicing reaction between splice sites in the target and PTM, splicing the C terminus portion of hRLuc adjacent to the N terminus portion, thus creating full-length *Renilla* luciferase (Fig. 2*C*).

The structures of LucHPVT3 and LucPTM37, as well as the proposed trans-splicing scheme between the two, are illustrated in Fig. 2. Both the target-expressing plasmid, pcLucHPVT3, and PTM-expressing plasmid, pcLucPTM37, were produced by ligating PCR-amplified fragments into the pcDNA3.1(−) vector backbone (Invitrogen). For the target plasmid, an 886-bp DNA fragment containing the N terminus portion of the humanized *Renilla* luciferase (hRLuc) was PCR-amplified from the phRL-SV40 vector (Promega). The primers used to produce the N terminus hRLuc insert were synthesized as follows: (Luc-16F) 5′-C TAG **GCT AGC** ATG GCT TCC AAG GTG TAC GAC CCC G, a 35-mer upstream primer introducing an *Nhe*I site (in bold) and with the underlined region homologous to nucleotides 1–24 of the hRLuc gene; (Luc-37R) 5′-C TAG **GGA TCC** *ACT TAC* CAC GAA GCT CTT GAT GTA CTT ACC CAT TTC, a 46-mer downstream primer introducing a *Bam*HI site (in bold) with the underlined region complementary to nucleotides 856–886 of the hRLuc gene and the italicized region coding for a 5′ donor site. Likewise, a 655-bp DNA fragment corresponding to portions of the E6 and E7 oncoproteins from human papillomavirus (HPV) type 16 was generated by using primers: (Luc-19F) 5′-C TAG **GGA TCC** GAC TTT GCT TTT CGG GAT TTA TGC, a 34-mer upstream primer introducing a *Bam*HI site (in bold) with the underlined region homologous to nucleotides 233–246 of the HPV gene target; (Luc-20R) 5′-C TAG **AAG CTT** TTA CTG CAG GAT CAG CCA TGG TAG, a 34-mer downstream primer introducing a *Hin*dIII site (in bold) with the underlined region containing a stop codon and complementary to nucleotides 866–880 of the HPV gene target. After amplification, the hRLuc PCR product was digested with *Nhe*I and *Bam*HI. Similarly, the HPV PCR product was digested with *Bam*HI and *Hin*dIII, and the pcDNA3.1(−) vector was digested with *Nhe*I and *Hin*dIII. The products of all three digestions were gel purified and then ligated to generate pcLucHPVT3.

To construct the PTM-expression plasmid, a 50-bp DNA fragment containing the C terminus portion of the hRLuc gene was PCR-amplified by using the following primers: (Luc-22F) 5′-C TAG **GAT ATC** *CAG* GTA AGT ACA TCA AGA GCT TCG, a 34-mer upstream primer introducing an *Eco*RV site (in

bold) with the underlined region homologous to nucleotides 887–907 and the italicized region introducing a 3′ splice acceptor site; (Luc-23R) 5′-C TAG **AAG CTT** TTA CTG CTC GTT CTT CAG CAC, a 31-mer downstream primer introducing a *Hin*dIII site (in bold) with the underlined region complementary to nucleotides 916–936 of hRLuc. To assemble the elements necessary for trans-splicing to occur (i.e., binding domain, spacer, branchpoint, and polypyrimidine tract) without any extraneous nucleotides, oligonucleotides were synthesized with *Nhe*I and *Eco*RV restriction sites at the 5′ and 3′ ends, respectively. The synthetic oligos were annealed by heating to 95°C and then allowed to cool to room temperature. The annealed oligos and hRLuc fragment were then ligated into an *Nhe*I- and *Eco*RV-digested pcDNA3.1(−) vector to generate pcLucPTM37.

Cell Culture and Transfections. Neuro-2a (N2a) mouse neuroblastoma cells were maintained in DMEM, supplemented with 10% FCS and 1% penicillin-streptomycin. To assess the ability of LucPTM37 to trans-splice into LucHPVT3, N2a cells were plated in 12-well plates, 60-mm dishes, or 100-mm dishes. Twenty-four hours later, the cells were transiently transfected with either pcLucHPVT3 or pcLucPTM37, or cotransfected with both pcLucHPVT3 and pcLucPTM37 by using SuperFect Transfection Reagent (Qiagen, Valencia, CA). Cells transfected with pCMV-hRL (Promega) were used as the positive control and mock-transfected cells were used as the negative control.

Luminometer Measurements. All bioluminescence assays were performed by using a TD 20/20 luminometer (Turner Designs, Sunnyvale, CA). Cells transfected in 12-well plates were lysed by using passive lysis buffer (Promega). Five microliters of cell lysate were mixed with 100 μl of coelenterazine (1 μg/ml in sodium phosphate buffer), and the reaction was measured in relative light units (RLU) over 10 s in the luminometer. Protein content of the cell lysate was measured by using Bio-Rad protein assay reagent (Bio-Rad Laboratories, Hercules, CA) in a Beckman DU-50 spectrophotometer (Beckman Coulter, Fullerton, CA), and luminescence results were reported as RLU per μg of protein per second.

Detection of Trans-Spliced Products by RT-PCR. To confirm that the intact hRLuc message was produced by trans-splicing, total RNA was isolated from cells transfected in 60-mm dishes or excised organs by using the RNeasy kit (Qiagen). RT-PCR was performed by using the EZ r*Tth* RNA PCR kit (Applied Biosystems) using 200 ng of total RNA and 100 ng each of the following primers designed to span the splice junction of the repaired hRLuc gene: (Luc-42F) 5′-GGA TAT CGC CCT GAT CAA GAG; or (Luc-41R) 5′-CTG CTC GTT CTT CAG CAC GCG. RT-PCRs were performed by using a PTC-200 Thermal Cycler (MJ Research, Reno, NV) and the following protocol: 60°C for 45 min, 94°C for 1 min, 35 cycles of 94°C (1 min), 48°C (1 min), 72°C (1 min), and a final extension step at 72°C for 15 min. The products were analyzed by gel electrophoresis using 2% agarose gels and stained with ethidium bromide. To confirm their identity, PCR bands were excised from the gels and sequenced by the UCLA Sequencing and Genotyping Core (University of California, Los Angeles).

Introduction of Transiently Transfected Cells Into Mice. All animal handling was performed in accordance with the University of California Los Angeles Animal Research Committee guidelines. Twenty-four hours after transfection, cells were collected by trypsinization, washed with PBS, counted, and then resuspended in PBS. Nude mice, ≈24 g in weight and 4 weeks old (Charles River Breeding Laboratories) were anesthetized by i.p. injections of ≈10 μl of a ketamine/xylazine (4:1) solution. After anesthetization, cells transiently transfected with pcLucHPVT3 (5×10^6 cells, suspended in 100 μl of PBS) or mock-transfected cells were implanted s.c. on the left and right side, respectively, of each animal's back ($n = 6$). Alternatively, mice were injected via the tail vein with cells (1×10^6 cells, suspended in 100 μl of PBS) transiently transfected with pcLucHPTV3 ($n = 8$) or mock-transfected cells ($n = 3$).

***In Vivo* Tf-PEI/DNA Polyplex Delivery of LucPTM37 to Mice.** The use of PEI polycation components for gene delivery has been described (12). Briefly, PEI components consisting of Tf-PEI25 and PEI22 (graciously provided by E. Wagner, Boehringer Ingelheim) were mixed in HBS buffer (75 mM NaCl/20 mM Hepes, pH 7.3) with 50 μg of pcLucPTM37 and incubated at room temperature for 20 min. Before injection, the complexes were adjusted with a 2.5% glucose solution to ensure physiologic iso-osmolarity. For the animals in which target-expressing cells were s.c. implanted, Tf-PEI-PTM37 complexes were injected via tail vein 24 h after target cell implantation and then scanned 24 h after Tf-PEI-PTM37 injection. For the animals in which target-expressing cells were injected intravenously, a subset ($n = 3$) was injected via tail vein with a single dose (1 dose = 50 μg pcLucPTM37) of the Tf-PEI-PTM37 complexes 4 h after cell injection. A second subset ($n = 3$) was injected with two doses, the first occurring 4 h after cell injection, and the second occurring 24 h after administration of the first dose. Both subsets of mice were scanned at 24, 48, and 72 h after the initial PTM injection. One subset ($n = 2$) of mice injected intravenously with target-expressing cells were scanned without being administered the Tf-PEI-PTM37 complexes to determine background levels of luminescence.

Imaging and Quantification of Bioluminescence. For small animal bioluminescence imaging, a Xenogen *in vivo* Imaging System (IVIS) (Xenogen, Alameda, CA) was used. Immediately before scanning, animals were anesthetized as before, and then injected via tail vein with coelenterazine (2.1 mg/kg of body weight). Animals were then placed directly in the imaging chamber, and whole body images were acquired for 5 min. Regions of interest (ROI) of constant area were manually drawn over areas of signal intensity by using the LIVING IMAGE software (Xenogen) and results were reported as maximum intensity values within an ROI in photons per second per cm^2 per steridian (sr).

Results

Reporter Gene Activity Is Restored by Trans-Splicing in Cell Culture. To evaluate the efficiency of the trans-splicing reaction, cells were transiently transfected with a plasmid expressing the pre-mRNA target, pcLucHPVT3, a plasmid expressing the PTM, pcLucPTM37, or both at a 1:1 ratio. Cells transfected with only the target or PTM plasmid showed minimal bioluminescence over background levels, indicating that cis-splicing of the target pre-mRNA does not result in functional *Renilla* luciferase and that the portion of hRLuc contained in the PTM is not sufficient for bioluminescent activity. When cells were cotransfected with both the target and PTM, a substantial gain in signal was observed. This strongly suggests that LucPTM37 is able to trans-splice into the LucHPVT3 pre-mRNA and reconstitute fully active *Renilla* luciferase. The luciferase signal produced by trans-splicing was compared against the signal from cells transfected with a plasmid coding for constitutively expressed full length hRLuc (pCMV-hRL) to estimate the efficiency of trans-splicing. Analysis revealed that the signal obtained from trans-splicing in cells co-transfected with both LucHPVT3 (target) and LucPTM37 (PTM) is ≈22–29% of the signal obtained from cells constitutively expressing full length hRLuc (Fig. 3A). As both the target pre-mRNA and PTM are under control of the CMV promoter, the pCMV-hRL control allows us to reasonably approximate trans-splicing efficiency. However, it is important

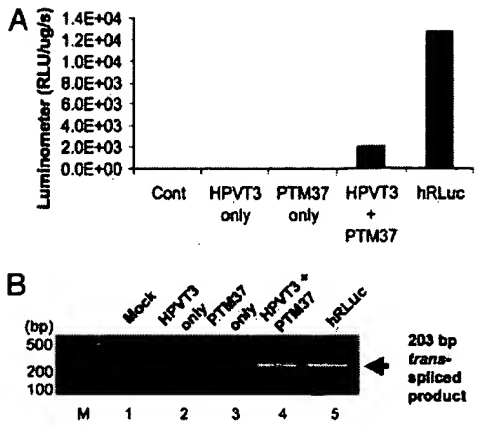

Fig. 3. mRNA repair and restoration of Luciferase function in cells. (*A*) Luminometer results reflecting the bioluminescence produced from hRLuc, generated by either the SMaRT trans-splicing reaction between HPVT3 and PTM37 or constitutively expressed full-length hRLuc. (*B*) RT-PCR results of fragments amplified by primers specific for opposite sides of the junction created by trans-splicing (lane 4). No evidence of trans-splicing was detected in mock-transfected cells or in cells transfected with plasmids expressing either target or PTM only (lanes 1–3).

to note here that this is not a measurement of trans-splicing efficiency alone. Rather, this estimation is a function, not only of trans-splicing efficiency, but also includes the transfection and transcriptional efficiency of the two plasmid system.

Little to no luciferase signal above background levels was detected in cells cotransfected with LucHPVT3 and a splice incompetent PTM that lacks functional 3′ splice elements (data not shown). These results further confirm that the luciferase signal observed in cotransfected cells is caused by trans-splicing between target pre-mRNA and PTM and is not caused by complementation of luciferase peptides separately expressed by the target and PTM.

RT-PCR Confirms Trans-Splicing Between Target Pre-mRNA and PTM in Cells. RT-PCR was performed to demonstrate that PTM-mediated trans-splicing generated full-length hRLuc transcripts. Twenty-four hours after transfection, total RNA was isolated from the cells, and hRLuc transcripts were amplified by RT-PCR with primers specific to opposite sides of the splice junction. Thus, only the products of trans-splicing reactions were amplified. Performing RT-PCR with primers Luc-42F/Luc-41R by using RNA isolated from cells expressing LucHPVT3 and LucPTM37 produced a product of 203 bp, which matched with the predicted product size generated with the same primers using RNA from cells transfected with pCMV-hRL (Fig. 3*B*, lanes 4 and 5). No specific product was detected in mock-transfected cells or in cells transfected with target or PTM only (Fig. 3*B*, lanes 1–3).

Trans-Splicing Can Be Imaged in Living Mice. Two experimental approaches were pursued to demonstrate that molecular imaging by trans-splicing could be achieved in living subjects. The first used s.c. implanted target-expressing cells as tumors in nude mice. A total of 5×10^6 N2a cells were transiently transfected with pcLucHPVT3 or mock transfected and then implanted bilaterally on the dorsal sides of mice ($n = 6$). Twenty-four hours after implantation, Tf-PEI-PTM37 polycation complexes were injected into the mice via the lateral tail-vein by using a poly(ethyleneimine) delivery system described elsewhere (12). Briefly, these polycation compounds complex with DNA because of their mutually attractive electric charges. By complexing

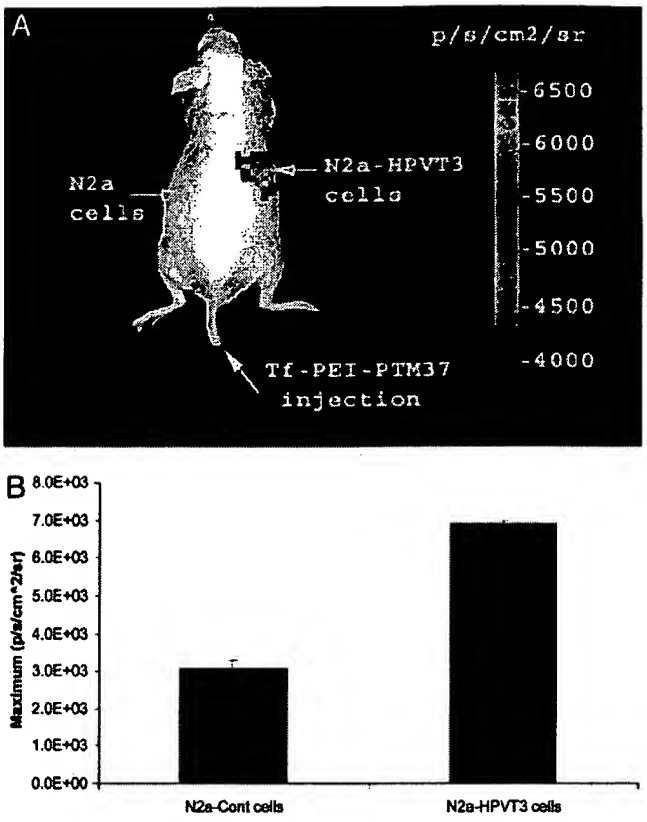

Fig. 4. Optical imaging of s.c. tumors in living mice using SMaRT. (*A*) Cells transfected with the pre-mRNA target LucHPVT3, or mock transfected were implanted s.c. onto different sides of a living mouse as shown. Twenty-four hours later, the mouse was injected with the Tf-PEI-PTM37 complexes via lateral tail vein, and then, 24 h after that, the mice were injected with coelenterazine and imaged by using a charge-coupled device camera. (*B*) ROI analysis of the maximum bioluminescent signal emitted from control and target-expressing tumors.

transferrin with the polycations, these compounds can selectively deliver DNA to cancer cells, which overexpress transferrin receptors. Twenty-four hours after PTM delivery, the mice were injected with coelenterazine and imaged by using a charge-coupled device (CCD) camera. As seen in Fig. 4*A*, the tumor site expressing the LucHPVT3 target emitted a detectable bioluminescent signal after LucPTM37 delivery. ROI analysis revealed that the signals from target-positive tumors are 2-fold greater than the background bioluminescence emitted from control tumors (Fig. 4*B*).

In the second approach, we examined whether trans-splicing could be observed in deeper tissues. To this end, we injected 1×10^6 N2a cells, transiently transfected with pcLucHPVT3, via the lateral tail vein into nude mice. Four hours after lateral tail-vein injection of the target-expressing cells, the Tf-PEI-PTM37 complexes were also injected via tail vein. Mice were then injected with coelenterazine substrate and scanned before PTM delivery and then again at 24, 48, and 72 h after LucPTM37 injection. Although it was predicted that the N2a-HPVT3 cells would become lodged in the lungs after i.v. administration, it was observed that bioluminescence was primarily emitted from the liver, before (Fig. 5*A*) and after (Fig. 5*B*) delivery of LucPTM37. This suggests that the N2a-HPVT3 cells travel throughout the vasculature until ultimately becoming lodged in hepatic tissue. Max-value ROI analysis revealed that the background bioluminescence produced by the N2a-HPVT3 cells in the liver is 1.1 ×

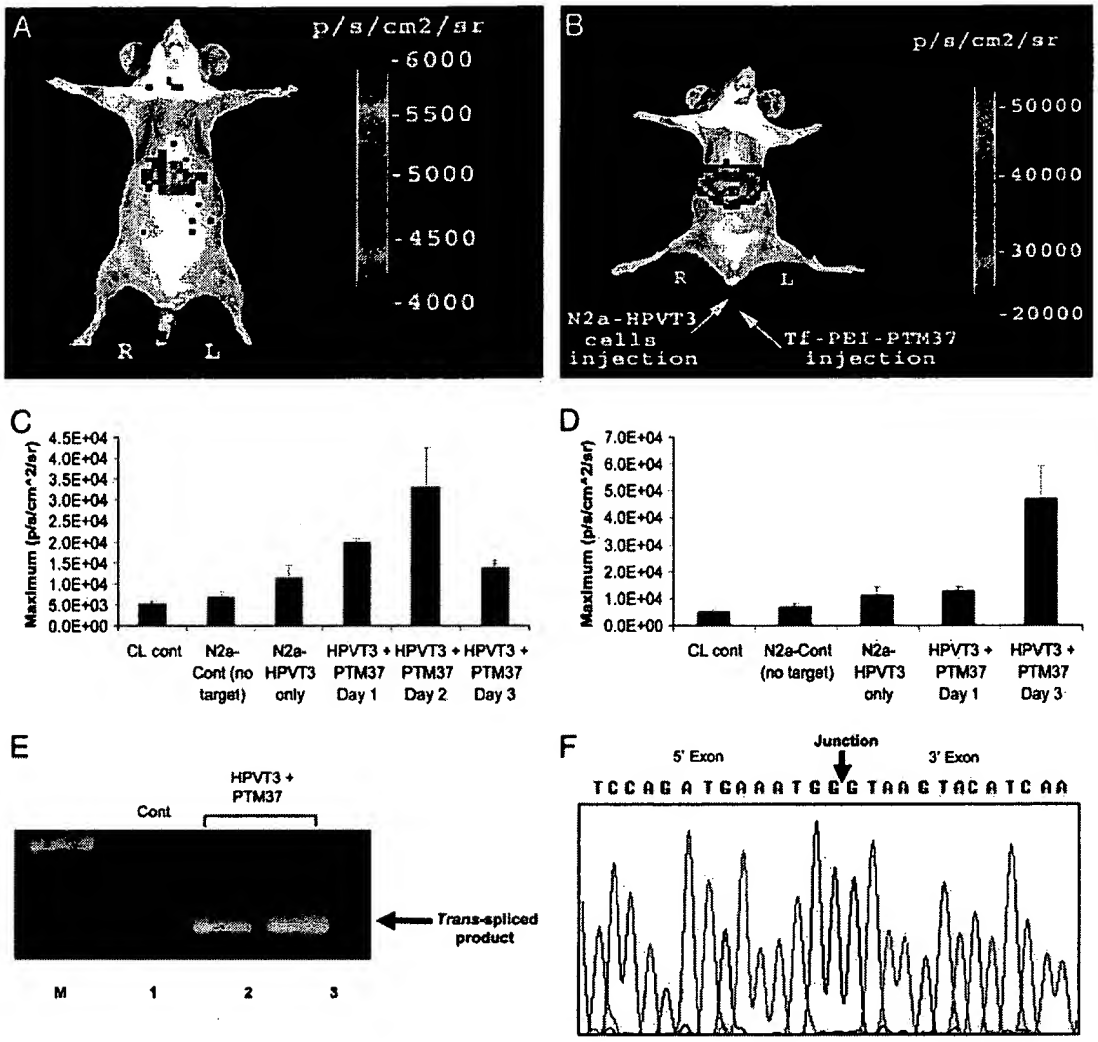

Fig. 5. Optical cell trafficking imaging using SMaRT. (*A*) Background bioluminescence produced by cells transiently transfected with LucHPVT3 and injected into a living mouse via the tail vein. (*B*) Bioluminescence observed in the same mouse seen in *A*, 48 h after injection of Tf-PEI-PTM37 complexes. (*C*) ROI analysis of bioluminescent signals emitted as a function of time after PTM-injection. The signal peaks at 2 days after injection and then subsides by day three. (*D*) Effects of multiple PTM-injections as assessed by ROI. Maximum signal is achieved by injecting a second PTM dose 24 h after the first PTM dose, and then imaging 48 h after the final injection. (*E*) RT-PCR results using total RNA isolated from the liver of mice injected with either zero (lane 1), one (lane 2), or two (lane 3) doses of Tf-PEI-PTM37 and using primers specific for opposite sides of the junction created by trans-splicing. (*F*) Sequencing results of RT-PCR products seen in *E*. Sequence analysis confirmed that the bands produced by RT-PCR are identical to the hRLuc sequence.

$10^4 \pm 3.0 \times 10^3$ p/s/cm^2/sr (Fig. 5*C*). After a single dose of LucPTM37, the maximum signal was observed at 48 h ($3.3 \times 10^4 \pm 9.3 \times 10^3$ p/s/cm^2/sr) and then subsided by 72 h after injection ($1.3 \times 10^4 \pm 1.7 \times 10^3$ p/s/cm^2/sr) (Fig. 5*C*). In an attempt to maximize the signal, we studied the effect of multiple doses of LucPTM37. A subset of mice injected intravenously with N2a-HPVT3 cells was given two doses of LucPTM37, with the first dose administered 4 h after target cell delivery, and the second dose given 24 h after the first (Fig. 5*D*). Max-value ROI analysis revealed that, within 48 h after the second LucPTM37 dose, the bioluminescent signal from the liver ($4.7 \times 10^4 \pm 1.7 \times 10^3$ p/s/cm^2/sr) was ≈1.4-fold greater than highest signal observed in the mice given only a single PTM dose (Fig. 5*D*).

RT-PCR Confirms Trans-Splicing in Living Mice. To confirm that the bioluminescent signals observed from the livers of the mice injected intravenously with N2a-HPVT3 cells were produced by trans-splicing, RT-PCR was performed on total liver RNA by using target- and PTM-specific primers as described above. RT-PCR analysis revealed the expected 203-bp product only in mice injected with LucPTM37 (Fig. 5*E*, lanes 2 and 3), but not from control mice injected only with target-expressing cells (Fig. 5*E*, lane 1). Direct sequencing of the product demonstrated the correct full-length hRLuc sequence, thereby confirming the accuracy of trans-splicing (Fig. 5*F*).

Discussion

SMaRT technology has been demonstrated to be a powerful and promising tool for gene therapy (13). Coupled with molecular imaging, it also has potential as a diagnostic platform to image gene expression (5). We have demonstrated in this report that the products of trans-splicing can be imaged in living animals, not only in s.c. tumors, but also in deeper tissues such as the liver. Although the model system provided here is not immediately applicable to universal imaging of any arbitrary mRNA target, our work presents an important step toward that goal.

Until now, attempts at imaging endogenous mRNA *in vivo* have met with limited success. A number of efforts have been

made to image endogenous genes with RASONs (14, 15). These molecules are generally modified nucleic acids (e.g., phosphorothioates, 2′-OMe backbone, peptide nucleic acids) that have been labeled with a radioisotope (e.g., F^{18}, In^{111}, Tc^{99m}). The principle behind imaging with RASONs is straightforward; a RASON can be designed to target an arbitrary sequence, then delivered systemically. The RASON will distribute throughout the organism and bind to the target sequence. Excess RASONs are eliminated from the organism, and the residual image reflects the location and level of expression of the gene of interest. The applicability of these molecules for imaging gene expression, however, is limited by their pharmacological properties. RASONs encounter several obstacles before reaching their targets, including degradation by nucleases and cellular impermeability. They also have nonspecific interactions and do not always efflux well from cells that do not contain the target mRNA.

The use of SMaRT technology and PTMs bypasses some of these hurdles because the targeting and reporter molecules are genetically encoded. Thus, SMaRT imaging can be reduced to a problem of gene delivery. To use gene delivery to accomplish global imaging of a particular gene's expression, care must be taken in choosing an appropriate vehicle for delivery as well as promoter for expression. If either the vehicle or the promoter chosen have distinct properties in various tissues, the results of such an image might obscure the true underlying biological processes. Using a constitutive promoter, known to drive expression robustly in many different tissues (as was done in this study with the CMV promoter), evades one of these problems. Although the science of transgene delivery has not yet been perfected, significant progress has been made over the last several years. Delivering the reporter molecule as a transgene greatly reduces the number of variables in the equation, thus making the goal of imaging mRNA more feasible. Signal amplification is another advantage of using SMaRT to image mRNA, because multiple signals are generated for each trans-splicing event. A RASON can at most produce as many signals as there are isotopes linked per RASON, and this is usually a single isotope. However, when a PTM splices into its target, the reporter gene encoded can be translated into multiple copies of an enzyme, which, in the presence of its substrate, can produce thousands of signals. This signal amplification, coupled with the modularity of SMaRT that facilitates the targeting of a wide variety of endogenous mRNA and potentially allows the use of many different reporter genes (e.g., multimodality fusion reporter genes; ref. 16), makes this method for imaging mRNA significantly more attractive than previously described approaches. In the current work, we did not normalize for transfection efficiency because the vectors used are in the same backbone and of comparable size. Under these conditions, we have found that transfection efficiency only accounts for 5–7% of the observed differences (unpublished data).

This study represents an important proof-of-concept in the overall scheme of developing SMaRT as a platform technology to image endogenous genes. Although we did not image an endogenous mRNA, this work demonstrates that trans-splicing can be used to image gene expression in living subjects. The success of this work was aided by targeting an exogenous gene, driven by a strong, constitutive promoter, and further experiments will strive to image endogenous genes that may not have such high levels of expression. Future studies will have to explore sensitivity of this assay as a function of number of target mRNAs. To accomplish this task, we must better understand the rules necessary to design and create PTMs that are specific to any target mRNA sequence of interest, and can deliver a full-length reporter that remains inactive until trans-splicing occurs. Toward this end, we are developing a functional genetic screen to rapidly screen millions of different sequence combinations to identify optimal PTMs with improved specificity and efficiency. This high-throughput screen coupled with rational design should permit the rapid development of a probe for any mRNA of interest, to report on the localization and magnitude of its expression. The applications for such a tool could advance a number of imaging-related areas of investigation, such as cell traffic monitoring, *in vivo* drug screening, and more sensitive noninvasive real-time diagnostics. A more immediate use of this technology is imaging the event of trans-splicing itself. Pairing a full-length reporter gene with PTMs designed for therapeutic uses would give investigators the ability to correlate the degree of gene repair by SMaRT with the level of reporter gene expression. Thus, established methods of noninvasive imaging could be used to monitor the gene therapy provided by SMaRT with hardly any modification. Given its advantages over other methods for imaging mRNA *in vivo*, together with its applicability to other active areas of investigation, SMaRT has the potential for becoming an essential implement in the molecular imaging toolbox.

This work was supported by National Institutes of Health Grant R01CA82214-05 and Department of Energy Grant DE-FG02-03ER63687 (to S.S.G.).

1. Southern, E. M. (1975) *J. Mol. Biol.* **98**, 503–517.
2. Stephens, A. C. & Rivers, R. P. (2003) *Curr. Opin. Mol. Ther.* **5**, 118–122.
3. Joos, L., Eryuksel, E. & Brutsche, M. H. (2003) *Swiss Med. Wkly.* **133**, 31–38.
4. Puttaraju, M., Jamison, S. F., Mansfield, S. G., Garcia-Blanco, M. A. & Mitchell, L. G. (1999) *Nat. Biotechnol.* **17**, 246–252.
5. Otto, E., Temple, G. F. & McGarrity, G. J. (2003) *Current Drug Discovery*, 37–42.
6. Chao, H., Mansfield, S. G., Bartel, R. C., Hiriyanna, S., Mitchell, L. G., Garcia-Blanco, M. A. & Walsh, C. E. (2003) *Nat. Med.* **9**, 1015–1019.
7. Liu, X., Jiang, Q., Mansfield, S. G., Puttaraju, M., Zhang, Y., Zhou, W., Cohn, J. A., Garcia-Blanco, M. A., Mitchell, L. G. & Engelhardt, J. F. (2002) *Nat. Biotechnol.* **20**, 47–52.
8. Puttaraju, M., DiPasquale, J., Baker, C. C., Mitchell, L. G. & Garcia-Blanco, M. A. (2001) *Mol. Ther.* **4**, 105–114.
9. Massoud, T. F. & Gambhir, S. S. (2003) *Genes Dev.* **17**, 545–580.
10. Bhaumik, S. & Gambhir, S. S. (2002) *Proc. Natl. Acad. Sci. USA* **99**, 377–382.
11. Paulmurugan, R. & Gambhir, S. S. (2003) *Anal. Chem.* **75**, 1584–1589.
12. Hildebrandt, I. J., Iyer, M., Wagner, E. & Gambhir, S. S. (2003) *Gene Ther.* **10**, 758–764.
13. Garcia-Blanco, M. A. (2003) *J. Clin. Invest.* **112**, 474–480.
14. Touboul, M., Gauchez, A. S., D'Hardemare Adu, M., Lunardi, J., Deverre, J. R., Pernin, C., Mathieu, J. P., Vuillez, J. P. & Fagret, D. (2002) *Anticancer Res.* **22**, 3349–3356.
15. Dewanjee, M. K., Haider, N. & Narula, J. (1999) *J. Nucl. Cardiol.* **6**, 345–356.
16. Ray, P., Wu, A. M. & Gambhir, S. S. (2003) *Cancer Res.* **63**, 1160–1165.

nature medicine

Phenotype correction of hemophilia A mice by spliceosome-mediated RNA *trans*-splicing

Hengjun Chao[1,3], S Gary Mansfield[2,3], Robert C Bartel[2], Suja Hiriyanna[2], Lloyd G Mitchell[2], Mariano A Garcia-Blanco[2] & Christopher E Walsh[1]

Conventional gene therapy of hemophilia A relies on the transfer of factor VIII (FVIII; encoded by the *F8* gene) cDNA. We carried out spliceosome-mediated RNA *trans*-splicing (SMaRT) to repair mutant FVIII mRNA. A pre-*trans*-splicing molecule (PTM) corrected endogenous FVIII mRNA in *F8* knockout mice with the hemophilia A phenotype, producing sufficient functional FVIII to correct the hemophilia A phenotype. This is the first description of phenotypic correction of a genetic defect by RNA repair in a knockout animal model. Our results indicate the feasibility of using SMaRT to repair RNA for the treatment of genetic diseases.

Hemophilia A is a sex-linked bleeding disorder caused by deficiency of coagulation factor VIII[1]. FVIII protein, in a complex with factor IX, regulates the conversion of factor X to Xa. In the absence of FVIII, this conversion is markedly reduced, leading to a phenotype characterized by frequent spontaneous bleeding. Mildly affected patients (suffering from rare bleeding episodes) maintain FVIII levels ≥5% of normal[2]. The *F8* gene contains 26 exons; exons 1 to part of 14 encode the FVIII heavy chain and the remaining exons encode the light chain. The heavy and light chains, which are proteolytic products of full-length FVIII, assemble noncovalently to form a functional protein. $F8^{-/-}$ homozygous mutant mice (designated *F8* E16) were created by insertion of the neomycin resistance gene into exon 16 (ref. 3). No functional FVIII protein is detected in these animals as a result of the absence of FVIII light chains. Although reduced compared with wild-type littermates, *F8* mRNA isolated from the livers of *F8* E16 mice can be detected by RT-PCR[4]. The presence of *F8* transcripts makes hemophilia A a candidate target for gene therapy techniques that depend on RNA repair.

For the treatment of hemophilia A (and many other genetic disorders), it remains a challenge to achieve efficient delivery of an entire therapeutic gene and the regulatory elements necessary for appropriate gene expression. Messenger RNA repair may circumvent these problems, which are associated with the conventional methods of delivering full-length cDNA for gene therapy. *Trans*-splicing of group I ribozymes[5–7] and antisense oligonucleotides[8] have been used to reprogram mutant RNA. SMaRT, which exploits the native cellular splicing machinery, is a more versatile approach[9–11]. Spliceosome-mediated RNA repair is driven by PTMs that base-pair with a specific target pre-mRNA sequence, thereby promoting specific *trans*-splicing. PTMs encode the domains required for efficient *trans*-splicing and RNA reprogramming, and the spliceosome provides catalysis. SMaRT has been used to repair mRNA encoding mutant β-galactosidase[9] and the cystic fibrosis transmembrane conductance regulator (CFTR) *in vitro* and *in situ*[11]. More recently, this method of RNA repair has been shown to produce functional β-galactosidase[10] and partially restore chloride ion efflux in a CFTR system[12]. However, all of these studies were carried out in tissue culture cells or in bronchial xenografts[9,11,12]. Here we show for the first time that SMaRT can be used to repair mRNA in *F8* knockout mice and thus correct the hemophilia A phenotype.

To test the ability of SMaRT to repair mutant *F8* transcripts in *F8* knockout mice, a plasmid was designed to encode a PTM that specifically base-pairs with intron 15 of *F8* pre-mRNA (Fig. 1a). PTMs were designed to mediate *trans*-splicing with exon 15 of the endogenous *F8* transcript by delivering the coding sequences for exons 16–26 and a C-terminal CDC2 epitope tag (PSTAIRE) for protein identification[13] (Fig. 1b,c).

Here we show both transient and long-term SMaRT repair of *F8* mRNA, restoration of *F8* activity, improvement in coagulation deficiency and hemophilia phenotype correction in *F8* knockout mice. These results suggest the usefulness of this methodology in treating hemophilia A.

RESULTS

SMaRT restores FVIII activity *in vivo*

To test the efficacy of SMaRT *in vivo*, we first developed two PTMs designed to test FVIII *trans*-splicing. To maximize *trans*-splicing efficiency[10], the repair PTM consisted of a 125-nucleotide binding domain complementary to mouse *F8* intron 15, a spacer sequence and a strong 3′ splice site. These three domains (binding domain, spacer and 3′ splice site) are called the *trans*-splicing domain (TSD). We refer to this repair PTM as p*F8*-PTM1 (Fig. 1a); it is designed to initiate a *trans*-splicing event between the mutant target pre-mRNA in the knockout mouse and the PTM, to generate a repaired full-length mRNA (Fig. 1a). A second PTM (p*F8*-PTM1ΔTSD) lacking the TSD was constructed to be splicing-incompetent and served as a

[1]Department of Medicine, Mt. Sinai School of Medicine, New York, New York 10029, USA. [2]Intronn Inc., Gaithersburg, Maryland 20878, USA. [3]These authors contributed equally to this work. Correspondence should be addressed to C.E.W. (christopher-e.walsh@msnyuhealth.org).

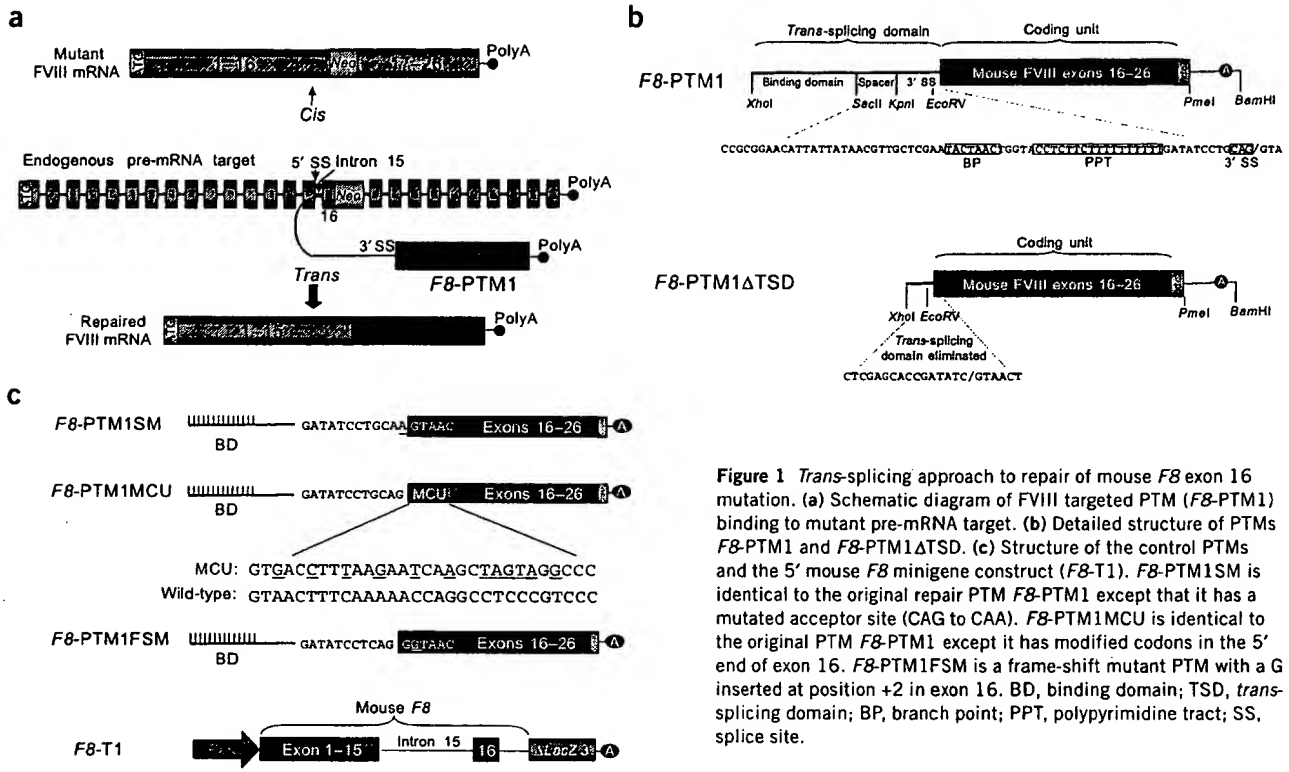

Figure 1 *Trans*-splicing approach to repair of mouse *F8* exon 16 mutation. (**a**) Schematic diagram of FVIII targeted PTM (*F8*-PTM1) binding to mutant pre-mRNA target. (**b**) Detailed structure of PTMs *F8*-PTM1 and *F8*-PTM1ΔTSD. (**c**) Structure of the control PTMs and the 5′ mouse *F8* minigene construct (*F8*-T1). *F8*-PTM1SM is identical to the original repair PTM *F8*-PTM1 except that it has a mutated acceptor site (CAG to CAA). *F8*-PTM1MCU is identical to the original PTM *F8*-PTM1 except it has modified codons in the 5′ end of exon 16. *F8*-PTM1FSM is a frame-shift mutant PTM with a G inserted at position +2 in exon 16. BD, binding domain; TSD, *trans*-splicing domain; BP, branch point; PPT, polypyrimidine tract; SS, splice site.

negative control (Fig. 1a). In both constructs, the mouse *F8* PTM is driven by the cytomegalovirus immediate-early enhancer linked to a modified chicken β-actin promoter. We directly administered 100 μg of p*F8*-PTM1 DNA into the hepatic circulation of *F8* E16 mice through the portal vein, a method that produces transient gene expression in mouse liver[14]. As expected for the delivery of naked DNA by this route, FVIII activity peaked at 48–72 h in the plasma of p*F8*-PTM1–treated mice (n = 9) and declined to baseline by day 7. Peak FVIII activity was as high as 20% of normal levels in individual animals, with a mean FVIII activity of 13% of normal (130.1 ± 54.4 mU/ml). No FVIII activity was detected in mice receiving control plasmid p*F8*-PTM1ΔTSD (<1% of normal FVIII activity; n = 5; Fig. 2a).

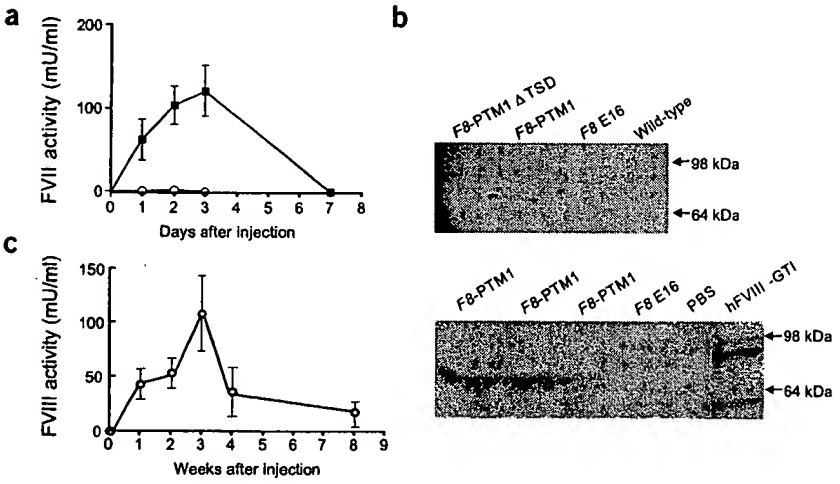

Figure 2 *Trans*-spliced mouse FVIII activity and antigen. (**a**) FVIII activity in the *F8* E16 mice injected with p*F8*-PTM1 (■; n = 9) or p*F8*-PTMΔTSD (○; n = 5). All samples were assayed in duplicate. (**b**) Western blot of FVIII light chain using antibody to PSTAIRE (human CDC2) epitope. Wild-type plasma was from wild-type C57BL/6 mice; hFVIII-GTI, plasma obtained from mice treated with an adenovirus vector carrying a human *F8* cDNA with a CDC2 PSTAIRE C-terminal epitope tag. (**c**) FVIII activity in *F8* E16 mice after injection of recombinant Ad*F8*-PTM1 (n = 10). All samples were assayed in duplicate.

To confirm that the FVIII activity was accompanied by the production of FVIII protein in p*F8*-PTM1–treated animals, western blot analysis was done on cryoprecipitated mouse plasma (Fig. 2b). In all four p*F8*-PTM1–treated mice that were tested with the antibody to human CDC2, we detected the expected ~70 kDa mouse FVIII light chain. No protein band was detected using plasma from untreated or control p*F8*-PTM1ΔTSD–injected *F8* E16 mice. To estimate the quantity of the mouse FVIII-CDC2-tagged protein, we used plasma obtained from mice treated with an adenovirus vector carrying a human *F8* cDNA with a CDC2 PSTAIRE C-terminal epitope tag. The activity of human FVIII-CDC2 in these samples was 800 mU/ml. Serial dilutions of cryoprecipitated plasma were run as standards (Fig. 2b). Mouse FVIII light chain is 70 kDa[4], whereas human FVIII light chain is 80 kDa[1]. Based on the band

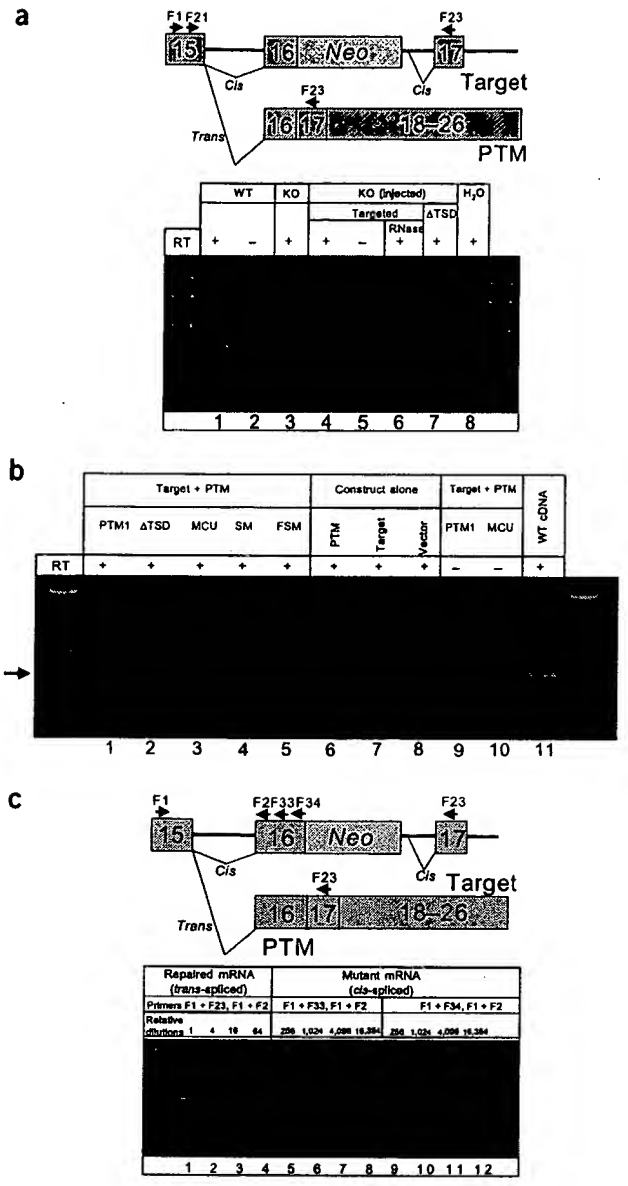

Figure 3 Quantitation of *cis*- and *trans*-spliced mouse *F8* mRNA. (a) Structure and detection of repaired *F8* pre-mRNA in the liver of a knockout mouse. Lanes 1, wild-type mouse; lane 2, wild-type mouse without reverse transcriptase; lane 3, noninjected knockout mouse; lanes 4–6, knockout mice injected with targeted PTM, with (lane 4) or without (lane 5) reverse transcriptase; lane 6, reaction with RNase A–treated DNA; lane 7, knockout mouse injected with control PTM; lane 8, water control. Only wild-type and knockout mice that received targeted PTM generated the appropriate band; all other reactions were negative. Spliced products (arrows) were generated using primers F21 and F23. (b) Detection of repaired *F8* pre-mRNA in 293 T cells. Lanes 1–5 are samples that received a PTM and target; lane 1, proof-of-concept repair PTM (*F8*-PTM1); lane 2, original splice mutant PTM (*F8*-PTM1ΔTSD); lane 3, repair PTM with exon 16 modified codons; lane 4, splice mutant PTM (*F8*-PTM1SM); lane 5, PTM that induces a frame-shift upon *trans*-splicing (*F8*-PTM1FSM); lanes 6–8, PTM, target or vector alone; lanes 9 and 10, samples that received one of two repair PTMs and a target but no reverse transcriptase; lane 11, sample that received wild-type *F8* cDNA. Spliced products (arrows) were generated using primers F1 and F23. Concentration of total RNA template in the RT-PCR reaction was 12.5 ng/μl. (c) Quantitation of *cis*- and *trans*-spliced *F8* mRNA, using total RNA from *F8* E16 mice injected with *F8*-PTM1. Primer pairs F1 + F33 or F1 + F34 were used in RT-PCR, followed by F1 + F2 in PCR. For *trans* products, we used F1 + F23 in RT-PCR followed by F1 + F2 in PCR. Primer pairs F1 + F33 and F1 + F34 will generate both *cis*- and *trans*-spliced products, so the final comparison is *trans*- versus *cis*- plus *trans*-. Primer pair F1 + F23 has never generated a product from RNA template isolated from a knockout mouse. RT, reverse transcriptase; WT, wild-type; KO, knockout; ΔTSD, *F8*-PTM1ΔTSD; PTM1, *F8*-PTM1; MCU, *F8*-PTM1MCU; SM, splice mutant; FSM, frame-shifting splice mutant.

intensities, we estimate that in the three p*F8*-PTM1–treated animals analyzed, we found the equivalent of ~100 mU/ml of CDC2 light-chain protein (Fig. 2b), which is consistent with our activity results. Recombinant adenoviruses carrying *F8*-PTM1 were used to further verify the generation of FVIII activity in *F8* E16 mice by the repair PTM (Fig. 2c)

FVIII activity results from repair of *F8* mRNA

To confirm that mutant *F8* transcripts were correctly *trans*-spliced to the PTM in mice injected with p*F8*-PTM1, we evaluated total RNA isolated from the liver by RT-PCR (Fig. 3a). RT-PCR and PCR experiments were done using primers specific for exon 15 (F1 and F21) in the endogenous target and exon 17 (F23) in the PTM. This reaction produced a single major product in samples from wild-type and knockout mice injected with p*F8*-PTM1 (Fig. 3a). The predicted size for a *trans*-spliced product between the endogenous target and the PTM is 276 base pairs. These products were subsequently shown by direct DNA sequencing to be *F8* in which exon 15 of the target was accurately *trans*-spliced to exon 16 of the PTM (data not shown). Controls were used to exclude contamination, PCR artifacts and DNA recombination events. Knockout mice injected with p*F8*-PTM1ΔTSD (which has no binding domain or splice elements) did not generate detectable *trans*-spliced RT-PCR products (Fig. 3a). No PCR products were detected in reactions where reverse transcriptase was eliminated for samples from normal or knockout mice. To assess whether products were generated through homologous recombination, we isolated RNase A–treated DNA from knockout mice injected with a targeted PTM and used this template in amplification reactions. Again, the reactions were negative for recombination products.

To further confirm that the repaired *F8* mRNA was indeed generated through the SMaRT reaction rather than plasmid DNA carryover, signature silent mutations were introduced at the 5′ end of exon 16 to make PTM p*F8*-PTM1MCU (Fig. 1c). RT-PCR detected *trans*-spliced product between the target p*F8*-T1 mRNA and the PTM mRNA after cotransfection of 293 cells with p*F8*-PTM1MCU (Fig. 3b). Direct sequencing of the RT-PCR products verified the accurate

Table 1 Correlation between FVIII activity and RNA *trans*-splicing

PTM	*F8*-PTM1	*F8*-PTM1ΔTSD	*F8*-PTM1SM	*F8*-PTM1MCU	*F8*-PTM1FSM
FVIII activity (mU/ml)	46.5 ± 1.9	2.8 ± 1.9	3.1 ± 0.8	38.1 ± 0.7	6.5 ± 1.5
Trans-splicing occurrence	+	–	–	+	+

Duplicate transfections were performed for each PTM tested. Culture media from each of the transfection samples was assayed for FVIII activity in triplicate. FVIII activity in untransfected cell media is <8 mU/ml

Table 2 Tail-clip challenge

	No. of mice	PTM dose (no. of viruses)	FVIII activity (mU/ml)	Tail-clip challenge (fraction survived)
C57BL/6 (wild-type)	5	NA	1,000	5/5
Naive *F8* E16	5	NA	<10	0/5
F8 E16 + Ad*F8*-PTM1ΔTSD	3	5×10^{10}	<10	0/3
F8 E16 + Ad*F8*-PTM1	10	5×10^{10}	24–215	8/10

Tail clip was done 3 weeks after injection of recombinant adenovirus vectors. Wild-type C57BL/6 mice ($n = 5$) were used as positive controls. The naive ($n = 5$) or Ad*F8*-PTM1ΔTSD–injected ($n = 3$) *F8* E16 mice were used as negative controls. NA, not applicable.

RNA *trans*-splicing between the exon 15 of the target construct and exon 16 of the PTM mRNA containing the signature silent mutations (data not shown). Up to 170.1 mU/ml of FVIII activity were measured in the supernatant from the p*F8*-PTM1MCU– and p*F8*-T1–transfected 293 cells (Table 1).

Normal FVIII protein processing requires that the primary FVIII polypeptide chain be proteolytically cleaved between Arg1648 and Glu1649 (located at the 3′ end of FVIII exon 14) to generate the FVIII light chain. Exon 15 encodes amino acid residues 1721–1772 and contains a thrombin/factor Xa cleavage site and a von Willebrand factor association site crucial for FVIII function. A mutation that skips exon 15 results in a severe hemophilia phenotype[15]. The PTM construct p*F8*-PTM1 encodes an in-frame translation product starting in exon 16. The p*F8*-PTM1 sequence contains no sequence homology to exons 14 or 15 and lacks the necessary thrombin cleavage site. It is unlikely that any functional product would result from a heavy chain *trans*-association to a light chain lacking exon 15. To completely rule out this possibility, however, a G-to-A mutation was introduced at the acceptor site of the construct p*F8*-PTM1SM, rendering it incapable of splicing (Fig. 1c). This mutation was also designed to maintain the same amino-acid coding as p*F8*-PTM1. We tested p*F8*-PTM1SM by cotransfecting 293 cells with a 5′ mouse *F8* minigene target construct (*F8*-T1) that expresses mutant mouse *F8* RNA transcripts similar to those in *F8* E16 mice (Fig. 1c). Cotransfection of 293 cells with the target plasmid p*F8*-T1 and p*F8*-PTM1SM did not produce detectable repaired mouse *F8* mRNA or FVIII activity, whereas cotransfection of p*F8*-PTM1 with the same target plasmid generated ~46.5 mU/ml of FVIII activity and repaired *F8* mRNA (Figs. 1c and 3b and Table 1). Injection of p*F8*-PTM1SM into the livers of *F8* E16 mice did not generate any detectable FVIII activity (<1% of normal FVIII activity; $n = 3$; data not shown).

The second PTM, p*F8*-PTM1FSM, is identical to the original proof-of-concept PTM (p*F8*-PTM1) but has a G inserted at the second base of the first codon in exon 16, a design feature that is intended to generate out-of-frame translation products in the presence of *trans*-splicing. This PTM, cotransfected with p*F8*-T1, produced a *trans*-spliced product (as would be expected) but no detectable FVIII activity (Fig. 3b and Table 1).

To estimate the number of mutant *F8* transcripts being converted to repaired transcripts through *trans*-splicing, we used semi-quantitative RT-PCR followed by a second round of PCR. RT-PCR was done with two different primer pairs for *cis*-spliced products and one pair for *trans*-spliced products. Samples for the first stage were taken in the range of linear amplification (28 cycles), column-cleaned, serially diluted and used in PCR reactions. Based on the intensity of the generated bands, we conservatively estimate that between 1.6 and 6.3% of mutant transcripts are being repaired (Fig. 3c; compare lanes 3 and 5 (16/256 or 6.25%) or lanes 3 and 6 (16/1024 or 1.6%)).

Genomic DNA was isolated from livers of mice 2 d after injection of p*F8*-PTM1. Southern blots were used to detect plasmid DNA. Dilutions of p*F8*-PTM1 were added to total genomic DNA isolated from untreated knockout mouse livers to serve as a quantification control. We detected 0.1–0.2 genome copies of p*F8*-PTM1 per cell, which is consistent with the efficiency of delivery reported by another group[16]. The vector genome numbers per cell in mice injected with p*F8*-PTM1 and p*F8*-PTM1ΔTSD were equivalent (data not shown).

SMaRT results in hemophilia A phenotype correction

To test for longer-term *F8* mutation correction and restoration of the hemophilia A coagulation deficit phenotype, we generated recombinant E1 element–deleted adenoviruses carrying the *F8*-PTM1 or the *F8*-PTM1ΔTSD cassette, and injected 5×10^{10} recombinant adenovirus virions into the tail veins of *F8* E16 mice. FVIII activity measured in the plasma of the Ad*F8*-PTM1–injected mice ($n = 10$) had a mean of 108.5 ± 35.3 mU/ml and peaked at 3 weeks after injection (Fig. 2c). FVIII activity in those mice was detected for up to 8 weeks after injection, although the levels declined to an average of 36.2 ± 22.7 mU/ml. FVIII activity in the plasma of the Ad*F8*-PTM1ΔTSD–injected mice was not detected ($n = 4$; data not shown). We then used the tail-clip assay 3 weeks after injection of recombinant Ad-PTM to test the hemostatic potential of these mice, which correlates to the severity of the hemophilia A phenotype. Eight of the ten mice that received a targeted PTM (Ad*F8*-PTM1) survived the tail-clip challenge, whereas none of the naive *F8* E16 (zero of five) or Ad*F8*-PTM1ΔTSD–injected (zero of three) mice survived the tail clip (Table 2). As a positive control, all of the five wild-type C57BL/6 mice survived the tail clip. These data show that RNA *trans*-splicing is capable of long-term *F8* repair and phenotype correction of the bleeding disorder in hemophilia A.

DISCUSSION

We have shown here that SMaRT can achieve mRNA repair and produce substantial levels of functional FVIII in *F8* knockout mice, thereby overcoming the coagulation deficit in hemophilic mice. For the treatment of many genetic disorders, SMaRT repair would obviate the need to deliver the entire normal gene coding sequence. The inability to deliver large genes, such as those mutated in cystic fibrosis[17] and Duchenne muscular dystrophy[18], hampers the genetic treatment of these disorders. By using the RNA *trans*-splicing strategy, replacement of only the mutated portion of the gene is required, which significantly reduces the transgene size required for gene packaging and delivery. Genes with large and complex transcriptional elements can be repaired *in situ*, leaving gene expression under the control of the endogenous regulatory elements. In addition, *trans*-splicing reduces the probability of ectopic gene expression, as production of repaired product is limited by the presence of the endogenous transcript. The specificity and efficiency of *trans*-splicing *in vivo* has not been fully determined, although the length and sequence of the *trans*-splicing binding domain significantly affects both specificity and *trans*-splicing efficiency[10]. The specificity of RNA *trans*-splicing technology needs to be more thoroughly evaluated; these studies are in progress. A report was recently published suggesting low specificity of *trans*-splicing, although this study used a short binding domain similar to the one used in our very early work[9,19]. More recent PTMs with longer binding domains have substantially improved specificity and efficiency[10].

Hemophilia A is a prime disease model for genetic correction. Here we have reported *in vivo* correction of the defective mouse *F8* gene by SMaRT, and the resultant correction of the hemophilia A phenotype. Our results suggest that RNA repair can be a general method for correcting inherited and acquired genetic diseases.

METHODS

Plasmid construction. Each PTM was assembled from a combination of PCR products, annealed oligonucleotides and subcloned vector fragments. All PCR products were generated with cloned Pfu DNA polymerase (Stratagene). The wild-type coding sequence for mouse FVIII exons 16–26 was PCR-amplified from a cDNA plasmid template (provided by H. Kazazian, University of Pennsylvania). PCR products were digested with the appropriate restriction enzymes and cloned into an existing PTM CF-PTM24 (ref. 10) containing a set of PTM splice elements. The splice elements included a spacer sequence, an extended polypyrimidine tract, a yeast branch-point consensus and a 3′ AG acceptor site. The PTM binding domain, complementary to nucleotides −142 to −29 and −6 to +4 of mouse FVIII intron 15 and exon 16, was generated by PCR from knockout mouse liver total genomic DNA.

Cell culture and plasmid transfection. HEK 293 T cells were transfected with plasmids using Lipofectamine Plus (Life Technologies). Duplicate transfections were done for each PTM tested. Culture media was recovered from each well of the six-well plates, centrifuged at 4,000 g for 4 min and stored at −80 °C until time of Coatest assay. FVIII activity was measured by Coatest as described below.

Animal procedures. The *F8* E16 mice were gifts from H. Kazazian (University of Pennsylvania)[3]. The mice were intrabred and maintained in accordance with the guidelines of the institutional Animal Care and Use Committee. Genotype of the *F8* E16 mice was verified by PCR and FVIII activity[3]. Recombinant adenovirus vectors were generated as previously described[20]. After anesthesia, intraportal injections of the plasmid or tail-vein injection of the recombinant adenovirus were done following the published protocol[14]. Approximately 20% (with plasmid injection) to 80% (with recombinant adenovirus injection) of the knockout mice survived the injection. Plasma of the injected mice was collected before and after injection by retro-orbital plexus bleeding. Tail-clip challenge was used to assess correction of the hemophilia phenotype as previously described[21].

FVIII activity and antigen assays. Mouse FVIII activity was assayed by Coatest (Chromgenix AB) according to the manufacturer's instructions, with minor modifications. Wild-type (C57BL/6) mouse plasma was added to naive *F8* E16 mouse plasma to generate a standard curve of mouse FVIII activity. All samples were done in duplicate. Mouse FVIII light-chain antigen was detected by western blot. Modified glycine cryoprecipitation was used to concentrate mouse FVIII from mouse plasma[4]. The cryoprecipitated FVIII (12 μl from 100 μl of plasma) was separated on 8% of precast glycine polyacrylamide gel (Novex) and transferred to nitrocellulose membrane. We detected the PSTAIRE epitope using rabbit antibody to human CDC2 kinase (PSTAIRE; 1:500 dilution; Upstate Biotechnology) combined with peroxidase-conjugated goat antibody to rabbit immunoglobulin (H+L; 1:1,000; Kirkegaard & Perry Laboratories). The signal was developed using a chemiluminescent Supersignal Substrate (Pierce).

Southern blot. Mouse liver genomic DNA was isolated as described previously[22]. Naive *F8* E16 mouse liver DNA was mixed with the plasmid p*F8*-PTM1 to generate the PTM genome copy number standard in hepatocytes. The DNA was digested with restriction enzyme *Bsp*EI (to linearize the plasmid) and then transferred to a nylon membrane. The PTM was detected with an α-^{32}P-labeled probe hybridized to the cytomegalovirus/chicken β-actin promoter sequence. The PTM copy number per cell in the treated mice was determined by PhosphorImager scanning of samples and standards.

RT-PCR and PCR. Total RNA or DNA was isolated from cultured cells or liver tissue using a MasterPure RNA/DNA purification kit (Epicenter Technologies). RT-PCR was done using an EZ-RT-PCR kit (Perkin-Elmer) as described previously[9]. The sequences of oligonucleotides F1 (exon 15), F21 (exon 15) and F23, used to generate *cis*- and *trans*-spliced products, are 5′-GGTATCAAAGTGACAATGTACC-3′, 5′-CCCATATATAAGAGCAGAAGTTG A-3′ and 5′-CCAATTAATCCCGAGTGCATATC-3′, respectively. Other oligonucleotides used in semi- quantitative *cis*- versus *trans*- comparisons were F2 (exon 16), F33 and F34, the sequences of which are 5′-GTTTCTTCTAGGTTCTTCTCCTC-3′, 5′-CTGACCTGCGGCCGCGTTTCTTCTAGGTT CTTCTCCTC-3′, and 5′-CTGACCTGCGGCCGCAGAGAAATAAGCCCAG GCCTTGC-3′, respectively. RT-PCR reactions were performed at 60 °C for 45 min, followed by 30 s of preheating at 94 °C, 25–35 cycles of PCR amplification at 94 °C for 18 s, annealing and extension at 60 °C for 45 s and a final extension at 72 °C for 7 min. In experiments where a second round of amplification was used, PCR was done with REDTaq DNA polymerase (Sigma) using the following conditions: one cycle of denaturation for 3 min at 94 °C, 25–30 cycles of denaturation at 94 °C for 30 s, annealing at 62 °C for 30 s, extension at 72 °C for 30 s and a final extension at 72 °C for 7 min. All reactions for RT-PCR and PCR were done under hot-start conditions.

ACKNOWLEDGMENTS

We thank J. Huang and X. Zeng for technical assistance, S. Connelly and P. Shirley (GTI/Novartis) for the Adhu*F8* mouse plasma and R. Sarkar and H. Kazazian for the *F8* E16 knockout mice and advice. H.J.C. is a recipient of a Career Development Award from the National Hemophilia Foundation. National Institutes of Health grant RO1-68215 provided funding for this project.

COMPETING INTERESTS STATEMENT

The authors declare competing financial interests (see the *Nature Medicine* website for details).

Received 30 April; accepted 16 June 2003
Published online 6 July 2003; doi:10.1038/nm900

1. Kaufman, R.J. & Antonarakis, S.E. Structure, biology, and genetics of factor VIII. in *Hematology: Basic Principles and Practice* Vol. VIII-108 (ed. McGlave, P.) 1850–1868 (Church Livingstone, New York, 2000).
2. Lillicrap, D. Hemophilia treatment. Gene therapy, factor VIII antibodies and immune tolerance: hopes and concerns. *Haematologica* **85**, 108–111 (2000).
3. Bi, L. *et al.* Targeted disruption of the mouse factor VIII gene produces a model of haemophilia A. *Nat. Genet.* **10**, 119–121 (1995).
4. Bi, L. *et al.* Further characterization of factor VIII-deficient mice created by gene targeting: RNA and protein studies. *Blood* **88**, 3446–3450 (1996).
5. Sullenger, B.A. & Cech, T.R. Ribozyme-mediated repair of defective mRNA by targeted, *trans*-splicing. *Nature* **371**, 619–622 (1994).
6. Sullenger, B.A. RNA repair as a novel approach to genetic therapy. *Gene Ther.* **6**, 461–462 (1999).
7. Watanabe, T. & Sullenger, B.A. RNA repair: a novel approach to gene therapy. *Adv. Drug Deliv. Rev.* **44**, 109–118 (2000).
8. Gorman, L., Mercatante, D. & Kole, R. Restoration of correct splicing of thalassemic beta-globin pre-mRNA by modified U1 snRNAs. *J. Biol. Chem.* **275**, 35914–35919 (2000).
9. Puttaraju, M., Jamison, S.F., Mansfield, S.G., Garcia-Blanco, M.A. & Mitchell, L.G. Spliceosome-mediated RNA *trans*-splicing as a tool for gene therapy. *Nat. Biotechnol.* **17**, 246–452 (1999).
10. Puttaraju, M., DiPasquale, J., Baker, C.C., Mitchell, L.G. & Garcia-Blanco, M.A. Messenger RNA repair and restoration of protein function by spliceosome-mediated RNA *trans*-splicing. *Mol. Ther.* **4**, 105–114 (2001).
11. Mansfield, S.G. *et al.* Repair of CFTR mRNA by spliceosome-mediated RNA *trans*-splicing. *Gene Ther.* **7**, 1885–1895 (2000).
12. Liu, X. *et al.* Partial correction of endogenous DeltaF508 CFTR in human cystic fibrosis airway epithelia by spliceosome-mediated RNA *trans*-splicing. *Nat. Biotechnol.* **20**, 47–52 (2002).
13. Roy, S. *et al. In vivo* evaluation of a novel epitope-tagged human factor VIII-encoding adenoviral vector. *Haemophilia* **5**, 340–348 (1999).
14. Budker, V., Zhang, G., Knechtle, S. & Wolff, J. Naked DNA delivered intraportally expresses efficiently in hepatocytes. *Gene Ther.* **3**, 593–598 (1996).
15. Yenchitsomanus, P. *et al.* Mutation causing exon 15 skipping and partial exon 16 deletion in factor VIII transcript, and a method for direct mutation detection. *Haemophilia* **7**, 335–338 (2001).
16. Herweijer, H. *et al.* Time course of gene expression after plasmid DNA gene transfer to the liver. *J. Gene. Med.* **3**, 280–291 (2001).
17. Koehler, D.R., Hitt, M.M. & Hu, J. Challenges and strategies for cystic fibrosis lung gene therapy. *Mol. Ther.* **4**, 84–91 (2001).
18. Karpati, G. & Acsadi, G. The principles of gene therapy in Duchenne muscular dystrophy. *Clin. Invest. Med.* **17**, 499–509 (1994).
19. Kikumori, T., Cote, G.J. & Gagel, R.F. Promiscuity of pre-mRNA spliceosome-mediated *trans* splicing: a problem for gene therapy? *Hum. Gene Ther.* **12**, 1429–1441 (2001).
20. He, T. *et al.* A simplified system for generating recombinant adenoviruses. *Proc. Natl. Acad. Sci. USA* **95**, 2509–2514 (1998).
21. Chao, H., Monahan, P., Liu, Y., Samulski, R. & Walsh, C. Sustained and complete phenotype correction of hemophilia B mice following intramuscular injection of AAV1 serotype vectors. *Mol. Ther.* **4**, 217–222 (2001).
22. Chao, H., Mao, L., Bruce, A. & Walsh, C. Sustained expression of human factor VIII in mice using a parvovirus-based vector. *Blood* **95**, 1594–1599 (2000).

nature medicine

Trans-splicing repair of CD40 ligand deficiency results in naturally regulated correction of a mouse model of hyper-IgM X-linked immunodeficiency

Minoru Tahara[1], Robert G Pergolizzi[1], Hiroyasu Kobayashi[1], Anja Krause[2], Karsta Luettich[2], Martin L Lesser[3] & Ronald G Crystal[1,2]

X-linked immunodeficiency with hyper-IgM (HIGM1), characterized by failure of immunoglobulin isotype switching, is caused by mutations of the CD40 ligand (CD40L), which is normally expressed on activated CD4+ T cells. As constitutive expression of CD40L induces lymphomas, we corrected the mutation while preserving the natural regulation of CD40L using pre-mRNA *trans*-splicing. Bone marrow from mice lacking CD40L was modified with a lentivirus *trans*-splicer encoding the normal CD40L exons 2–5 and was administered to syngenic CD40L-knockout mice. Recipient mice had corrected CD40L mRNA, antigen-specific IgG1 responses to keyhole limpet hemocyanin immunization, regulated CD4+ T-cell CD40L expression after CD3 stimulation in primary and secondary transplanted mice, attenuation of *Pneumocystis carinii* pneumonia, and no evidence of lymphoproliferative disease over 1 year. Thus, HIGM1 can be corrected by CD40L *trans*-splicing, leading to functional correction of the genetic defect without the adverse consequences of unregulated expression of the CD40L gene.

HIGM1 is a rare, X-linked, recessive immunodeficiency disease characterized by failure of immunoglobulin isotype switching from IgM to IgG, IgA and IgE[1,2]. The disease is caused by mutations of the gene encoding CD40L, a cell surface ligand expressed by CD4+ T cells in an activation-mediated regulated fashion[3–5]. The functional effect of the mutations in the CD40L gene results in limitation of the interaction of the CD4+ T cells with the CD40 glycoprotein on the surface of B cells, macrophages and dendritic cells[6–8]. Because of this limited interaction, individuals with HIGM1 suffer from recurrent bacterial infections, especially with opportunistic microorganisms such as *P. carinii*[1,2]. Only 20–40% of individuals with HIGM1 reach the third decade of life[9,10]. At present, other than treatment for acquired infections, the only available therapy for HIGM1 is bone marrow transplantation[11,12].

As HIGM1 is a X-linked recessive disorder, the gene defect is known and the major phenotype is associated with a deficiency of CD40L in cells derived from bone marrow, gene therapy is an obvious approach to a potential cure for this disorder. The feasibility of using gene therapy for HIGM1 was demonstrated by Brown *et al.*[13] using *ex vivo* retrovirus-mediated CD40L gene transfer to bone marrow cells in a mouse CD40L-knockout model. Although this approach corrected the CD40L deficiency state and stimulated humoral and cellular immune functions, the mice developed T lymphoproliferative disease, suggesting that even a small amount of constitutive expression of CD40L can be risky, resulting in abnormal proliferative responses in developing T lymphocytes[13,14]. The experience of Brown *et al.*[13] using a constitutive promoter and the full-length normal CD40L cDNA suggests the need for regulated expression in gene therapy approaches to HIGM1 therapy[13,14].

Genetic repair strategies that preserve the natural regulation of genes may have therapeutic and safety advantages over traditional gene therapy approaches for the treatment of genetic disorders such as HIGM1 (ref. 15). One such approach is *trans*-splicing, a process by which two different pre-mRNAs are joined by the cellular splicing apparatus[16–22]. This mechanism, first discovered in trypanosomes and also seen in mammalian cells[23,24], has been developed as a strategy to correct mutant target mRNAs by splicing an exogenous mRNA into the normal portion of the mutated mRNA[16–22]. Theoretically, the major advantage of *trans*-splicing over conventional gene therapy is that the corrected genes can be maintained in their native sequence context and are regulated by their endogenous regulatory machinery. In the context of these considerations, the focus of our study is to demonstrate that *trans*-splicing can be used to correct the CD40L mutation while preserving the natural regulation and cell specificity of CD40L expression in a mouse CD40L-knockout model, enabling the mice to develop host defenses against *P. carinii* without the adverse effect of lymphoproliferative disease.

RESULTS

Trans-splicing corrects mutant CD40L mRNA *in vitro*

To optimize the specificity and efficiency of *trans*-splicing-mediated correction of mutated CD40L, we carried out preliminary *in vitro*

[1]Department of Genetic Medicine, [2]Belfer Gene Therapy Core Facility, Weill Medical College of Cornell University, New York, New York, USA. [3]Biostatistics Unit, North Shore–Long Island Jewish Research Institute, Manhasset, New York, USA. Correspondence should be addressed to R.G.C. (geneticmedicine@med.cornell.edu).

Published online 25 July 2004; doi:10.1038/nm1086

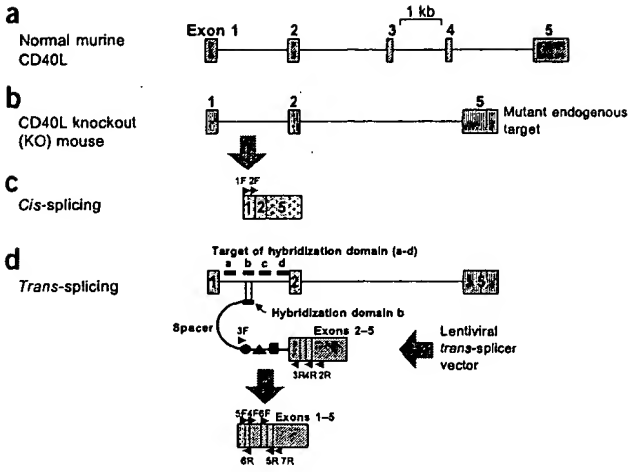

Figure 1 Schematic illustration of the strategy used for *trans*-splicing of CD40L mRNA *in vivo*. (**a**) Normal mouse CD40L pre-mRNA containing exons 1–5. (**b**) CD40L pre-mRNA from the CD40L-knockout mouse lacking exons 3 and 4. (**c**) *Cis*-splicing of the mutant CD40L pre-mRNA (shown in b) yields a mutant CD40L mRNA lacking exons 3 and 4. (**d**) Lentiviral-mediated expression of a *trans*-splicer expressing (5′ to 3′) hybridization domain, spacer, branch point (●), polypyrimidine tract (▲), splice acceptor (■) sequences and exons 2–5 of CD40L mRNA. The hybridization domain is antisense to a 312-bp sequence of intron 1 of CD40L pre-mRNA, allowing the *trans*-splicer to hybridize to the target pre-mRNA. The hybridization domains were targeted against four different regions in intron 1 of the CD40L pre-mRNA (labeled a–d). Domain b was the most efficient at promoting *trans*-splicing. *Trans*-splicing in this fashion connects exon 1 of target pre-mRNA and exons 2–5 of the *trans*-splicer transcript, and thus should yield a corrected mRNA. Arrowheads indicate the genomic PCR and RT-PCR primers for detection of *trans*-splicer transcripts and *cis*- and *trans*-spliced products.

experiments. HeLa cells were transfected with target plasmids encoding mutant CD40L (Fig. 1) together with plasmids encoding different *trans*-splicer constructs, each bearing a hybridization domain complementary to different regions of CD40L intron 1 (Full details of these *in vitro* experiments are described in Supplementary Note and Supplementary Figs. 1 and 2 online). A *trans*-splicer containing a 312-nucleotide hybridization domain targeted to a region beginning 432 nucleotides from the 5′ end of CD40L intron 1 (Fig. 1d, region 'b') was the most efficient construct tested *in vitro*, correcting 10.4% of total CD40L transcripts (Supplementary Fig. 2 online). This construct was used for all subsequent experiments.

Further *in vitro* experiments verified that *trans*-spliced CD40L was expressed on the surface of transfected HeLa cells, and was capable of stimulating B cell proliferation, IgE production and macrophage activation (Supplementary Note and Supplementary Fig. 3 online). *In vitro* translation experiments with *trans*-splicer mRNA suggested negligible peptide production from possible internal open reading frames (Supplementary Note online).

Lentivirus-mediated *trans*-splicing in CD40L-knockout mice

To evaluate the efficiency of *trans*-splicing *in vivo*, we constructed a lentivirus vector, LVtsCD40L2-5, encoding the same optimized expression cassette as used in the *in vitro* studies. Vector-transduced bone marrow cells (2×10^5) from CD40L-knockout mice were transplanted into lethally irradiated CD40L-knockout recipient mice (Figs. 1 and 2, and Supplementary Methods online). At 10 weeks after transplantation, we collected cells from the recipients and assayed for the presence of LVtsCD40L2-5 by genomic PCR, and for expression of the transgene by PCR with reverse transcription (RT-PCR). PCR analysis of genomic DNA from bone marrow cells isolated from CD40L-knockout *trans*-splicer recipient mice (Fig. 2a) revealed the anticipated 431-bp amplification product, indicating successful engraftment of the transduced cells. RT-PCR analysis (Fig. 2a) showed expression of the transgene in the transplanted mice. The presence of vector DNA and mRNA in peripheral blood cells (Fig. 2b) and spleen (Fig. 2c) was confirmed in the transplant recipients, demonstrating transduction of bone marrow cells, expansion of the transplant into these cellular compartments and expression of the CD40L *trans*-splicer transgene. In control experiments, LVeGFP (a lentivirus vector encoding enhanced green fluorescent protein) infection of bone marrow cells was used as an index of gene transfer, revealing that 20% of peripheral T cells were positive for eGFP 5 weeks after transplantation.

To demonstrate CD40L *trans*-splicing in the transplant recipients, we carried out RT-PCR on RNA from splenocytes isolated from *trans*-splicer-treated CD40L-knockout mice, using a CD40L *trans*-splicing-specific primer set (2F and 4R; Fig. 1) or a second primer set that amplified both *trans*- and *cis*-spliced CD40L mRNAs (1F and 3R; Fig. 1). RT-PCR on RNA isolated from LVtsCD40L2-5-treated CD40L-knockout mice (Fig. 2d) showed the expected 284-bp fragments indicating that *trans*-splicing had occurred. However, no amplification was seen in untreated CD40L-knockout mice (Fig. 2d, lane 24). All mice showed the RT-PCR product with the CD40L *trans* + *cis* primer set (Fig. 2d).

Sequencing of the RT-PCR products of *trans*-spliced CD40L revealed the correct splice junction sequence resulting from splicing events between endogenous target and *trans*-splicer transcripts, indicating that *trans*-splicing had occurred correctly *in vivo* with high fidelity. Quantitative RT-PCR of *trans*-spliced CD40L mRNA as a fraction of total CD40L mRNA was used as a measure of efficiency of *trans*-splicing and was determined to be 1.2% (mean).

To demonstrate that the corrected bone marrow cells provide for systemic therapy of HIGM1 and to confirm transduction of primitive hematopoietic cells, we carried out secondary transplantation of bone marrow cells collected from the 4-month-old CD40L-knockout recipient group in naive, lethally irradiated CD40L-knockout mice. Bone marrow cells were harvested from primary CD40L-knockout transplant recipients 4 months after the initial transplant and were transplanted to irradiated CD40L-knockout mice (secondary transplant recipients). At 6 weeks after secondary transplantation, peripheral blood cells from secondary transplant recipients were analyzed (Fig. 2e), showing the anticipated product in all transplant recipients. The average number of *trans*-splicer gene copies per splenic T cell, assessed by quantitative real-time PCR, was 0.27. These results demonstrate expansion of the transduced long-term repopulating compartment in the primary and secondary transplant recipients, suggesting the possibility of using this approach for systemic therapy for HIGM1.

Trans-spliced CD40L partially restores immunoglobulin switching

Previous reports indicated that CD40L-knockout mice fail to mount secondary antigen-specific responses to immunization with a thymus-dependent antigen, keyhole limpet hemocyanin (KLH)[25]. To assess the ability of *trans*-spliced CD40L to mediate the restoration of immunoglobulin subclass switching in mice, *trans*-splicer recipient CD40L-knockout mice were immunized with KLH. As a positive control, CD40L-knockout mice that had been previously transplanted with bone marrow cells from wild-type mice were used, and as a negative control, LVeGFP-treated CD40L-knockout mice and untreated CD40L-knockout mice were used. At 34 d after the first

immunization, we collected sera and measured KLH-specific antibodies by enzyme-linked immunosorbent assay (ELISA). RT-PCR was used to evaluate the *trans*-spliced mRNA products in the spleens of immunized mice arising from *trans*-splicing of CD40L mRNA (Fig. 2f). All mice immunized with KLH produced KLH-specific IgM (Fig. 3a). As expected, LVeGFP-treated knockout and untreated knockout mice did not produce KLH-specific IgG1. In contrast, *trans*-splicer-treated CD40L-knockout mice produced KLH-specific IgG1, demonstrating that *trans*-spliced CD40L partially restores humoral immunity *in vivo* ($P < 0.005$, knockout + *trans*-splicer versus knockout + LVeGFP or untreated knockout mice; Fig. 3b).

Regulated expression of *trans*-spliced CD40L *in vivo*

Theoretically, an advantage of *trans*-splicing-mediated correction of CD40L deficiency over conventional gene therapy is the potential to preserve natural regulation by targeting the endogenous mRNA, thereby preserving the normal regulation of mRNA for that gene. To determine whether the expression of *trans*-spliced CD40L in $CD4^+$ T cells was normally regulated, we collected splenic $CD4^+$ T cells from wild-type mice, *trans*-splicer-treated CD40L-knockout mice and untreated CD40L-knockout mice. $CD4^+$ T cells were activated by antibody to CD3, and CD40L expression was examined using flow cytometry at 0, 16, 40 and 64 h after activation. CD69 expression was examined as a marker of early activation of T cells[26]. As expected, almost all $CD4^+$ T cells in CD40L wild-type and CD40L-knockout mice expressed CD69 by 16 h after activation, suggesting uniform activation by the CD3 antibody (data not shown). Wild-type mice showed the anticipated pattern of CD40L expression in $CD4^+$ T cells after activation, with an increase to 69% positive for CD40L expression by 16 h and a decrease by 64 h (Fig. 4a). In a time-dependent pattern similar to that of wild-type $CD4^+$ T cells, $CD4^+$ T cells from *trans*-splicer-treated CD40L-knockout mice showed expression of CD40L increasing from 1% to 5.5% by 16 h after activation and then decreasing to baseline by 40 h (Fig. 4a). In contrast, $CD4^+$ T cells from untreated CD40L-knockout mice showed no increase in the expression of CD40L at any time. Peripheral blood T cells, B cells and granulocytes/monocytes were negative for expression of CD40L in *trans*-splicer-treated knockout mice (data not shown). These data are consistent with the concept that the expression of *trans*-spliced CD40L is normally regulated in activated $CD4^+$ T cells.

$CD4^+$ T cells from secondary transplant recipient CD40L-knockout mice (produced using the primary transplant recipients as donors) showed a pattern of expression of CD40L similar to that of cells from the primary transplant recipients, increasing from 1.9% to 5.0% by 8 h after activation, reaching 7.3% by 16 h and decreasing to baseline by 40 h (Fig. 4b). This confirmed the regulated expression of *trans*-spliced CD40L and the successful transduction and engraftment of long-term repopulating cells in the primary bone marrow cell population.

Attenuation of *P. carinii* infection in corrected knockout mice

To determine whether *trans*-spliced CD40L confers protection against *P. carinii* pneumonia in experimental mice, we injected 2×10^6 *P. carinii* organisms intratracheally into wild-type mice, *trans*-splicer-treated CD40L-knockout mice or LVeGFP-treated CD40L-knockout

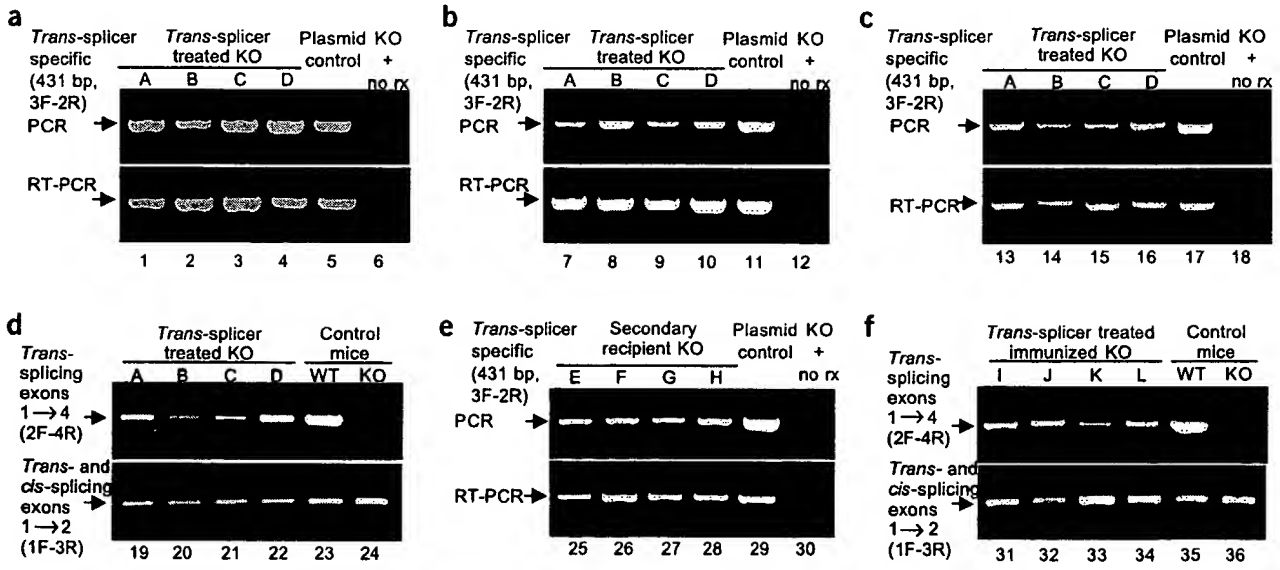

Figure 2 *Ex vivo trans*-splicing-mediated correction of CD40L pre-mRNA in CD40L-knockout mice. (**a**) Presence of the *trans*-splicer vector DNA in bone marrow and expression of *trans*-splicer mRNA *in vivo*. The primers were specific for the *trans*-splicer (3F-2R, **Fig. 1**). Top, PCR assessment for the presence of the *trans*-splicer DNA; bottom, RT-PCR for *trans*-splicer mRNA. Lanes 1–4, bone marrow from four (A–D) *trans*-splicer-treated CD40L-knockout mice; lane 5, *trans*-splicer plasmid as a control; lane 6, negative control of untreated CD40L-knockout marrow (no rx). (**b**) Peripheral blood cells, similar analysis to **a**. Lanes 7–12 are parallel to 1–6 in **a**. (**c**) Spleen, similar analysis to **a**. Lanes 13–18 are parallel to 1–6 in **a**. (**d**) Demonstration of correction of mutated CD40L by *trans*-splicing to produce a complete CD40L mRNA. Shown in both top and bottom panels are RT-PCR analysis of spleen mRNA in CD40L-knockout mice corrected with the *trans*-splicer. Top, exons 1–4 (corrected by *trans*-splicer only); bottom, exons 1–2 (representing uncorrected and corrected). Lanes 19–22, spleen from four (A–D) *trans*-splicer-treated CD40L-knockout mice; lane 23, spleen from wild-type mice; lane 24, spleen from knockout mice. (**e**) Peripheral blood cells from secondary transplant recipient mice (labeled E–H), analyzed as described in **a**. Lanes 25–28 show results for secondary transplant recipient mice; lanes 29 and 30 are controls as described in **a**. (**f**) Demonstration of correction of mutated CD40L by *trans*-splicing in immunized mice (labeled I–L), analyzed as described in **d**. Lanes 31–34 show results for immunized mice with KLH; lanes 35 and 36 are controls as described in **d**. In panels **a**, **b**, **c** and **e**, 'no rx' indicates untreated knockout mouse bone marrow (negative control).

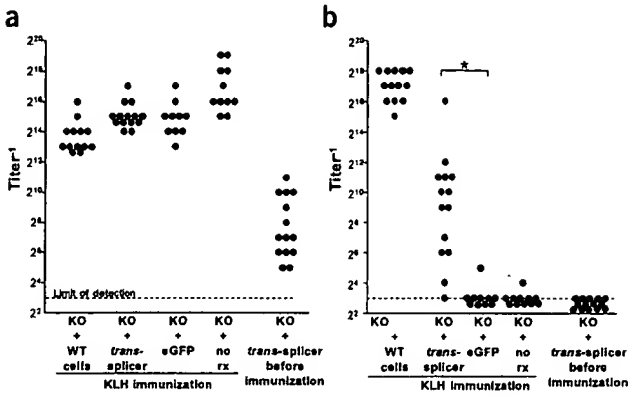

Figure 3 Partial restoration of immunoglobulin subclass switching mediated by *trans*-spliced CD40L in response to a thymus-dependent antigen (KLH) *in vivo*. (a) IgM-KLH-specific antibodies in serum measured by ELISA on day 34. KO, knockout; WT, wild type. (b) IgG1-KLH–specific antibodies at the same time. For **a** and **b**, each data point represents the titer of one mouse. Bone marrow cells from wild-type mice transplanted to CD40L-knockout mice (KO + wild-type cells, $n = 13$) were used as a positive control, and LVeGFP-treated CD40L-knockout mice (KO + eGFP, $n = 10$) and untreated CD40L-knockout ($n = 11$) as negative controls. $^*P < 0.005$, knockout + *trans*-splicer versus knockout + LVeGFP or untreated knockout mice.

mice. Wild-type controls were injected intratracheally with saline. Also at 8 weeks after injection, age-matched LVeGFP-treated CD40L-knockout mice showed decreased body weight (24.6 ± 0.8 g, mean ± s.e.m.) as compared with *trans*-splicer-treated mice (27.3 ± 0.5, $P < 0.01$ *trans*-splicer-treated versus LVeGFP-treated) and wild-type mice (29.9 ± 0.5), suggesting that LVeGFP-treated mice, but not *trans*-splicer-treated mice, developed *P. carinii* pneumonia.

Lung sections from LVeGFP-treated CD40L-knockout mice stained with hematoxylin and eosin (H&E) showed substantial accumulation of lymphocytes, some macrophages and giant cells, thickened alveolar septa and exudation of amorphous foamy material into many of the alveoli, suggesting severe pneumonia (data not shown). In contrast, lung sections from *trans*-splicer-treated CD40L-knockout mice showed limited evidence of inflammation. Lung sections from wild-type mice were similar to those of saline-injected control mice (data not shown). Thus, *trans*-spliced CD40L therapy attenuated inflammation in lungs of mice infected with *P. carinii*.

Consistent with these data, LVeGFP-treated CD40L-knockout mice showed substantial accumulation of Gomori methanamine silver (GMS)-stained organisms in the lungs (Fig. 5a). Under high magnification, GMS-stained organisms had a cystic structure and nucleus, indicative of *P. carinii* (Fig. 5b). In contrast, *trans*-splicer-treated mice showed a decreased area of GMS-stained organisms in alveoli (Fig. 5c). As expected, wild-type mice show very few GMS-stained organisms in alveoli (Fig. 5d). The saline-injected control mice had no GMS-stained organisms. These data illustrate the *trans*-spliced CD40L–induced attenuation of *P. carinii* infection. Consistent with these results, wet right lung weight decreased less in *trans*-splicer-treated mice than in LVeGFP-treated mice (0.15 g and 0.24 g, mean; $P < 0.005$ *trans*-splicer-treated knockout versus eGFP-treated control knockout; Fig. 5e), and *P. carinii* ribosomal RNA was reduced in *trans*-splicer-treated mice as compared with LVeGFP-treated mice (0.35 and 1, mean, $P < 0.005$ *trans*-splicer-treated knockout versus eGFP-treated control knockout; Fig. 5f), further indicating attenuated *P. carinii* infection.

Chronic *P. carinii* pneumonia in experimental mice results in the increased expression of interferon (IFN)-γ and tumor necrosis factor (TNF)-α in the lungs of CD4⁺-depleted mice[27,28]. Consistent with the histology and *P. carinii* quantitative data, *trans*-splicer-treated CD40L-knockout mice showed decreased IFN-γ in lung homogenates relative to LVeGFP-treated mice (mean, 45 pg/g tissue and 850 pg/g tissue, respectively; $P < 0.005$ *trans*-splicer-treated knockout versus eGFP-treated control knockout; Fig. 5g). Likewise, *trans*-splicer-treated CD40L-knockout mice showed decreased amounts of TNF-α

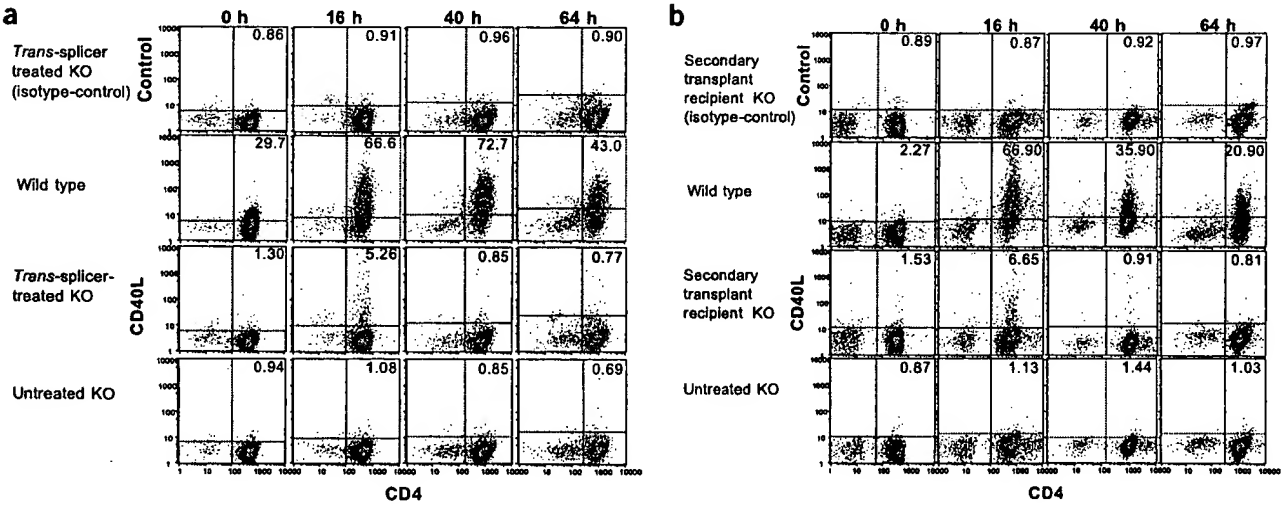

Figure 4 Analysis of CD40L expression in CD4⁺ T cells from CD40L *trans*-spliced mice. (a) Expression in CD4⁺ cells from CD40L-knockout transplant recipient mice. Splenocytes were harvested from *trans*-splicer-treated CD40L-knockout mice 2 months after bone marrow transplantation, from wild-type mice or from untreated CD40L-knockout mice. At 0, 16, 40 or 64 h after activation, CD4⁺ T cells were stained with allophycocyanin-labeled antibody to CD4 and phycoerythrin (PE)-labeled antibody to CD40L or PE-isotype control. Expression of CD4 and CD40L in CD4⁺ T cells was analyzed by flow cytometry. Percentage of CD4⁺CD40L⁺ cells are indicated in each panel. KO, knockout. (b) Expression in CD4⁺ cells from secondary transplant recipient mice. Splenocytes harvested from secondary transplant recipient CD40L-knockout mice 8 weeks after secondary bone marrow transplantation and analyzed as in a.

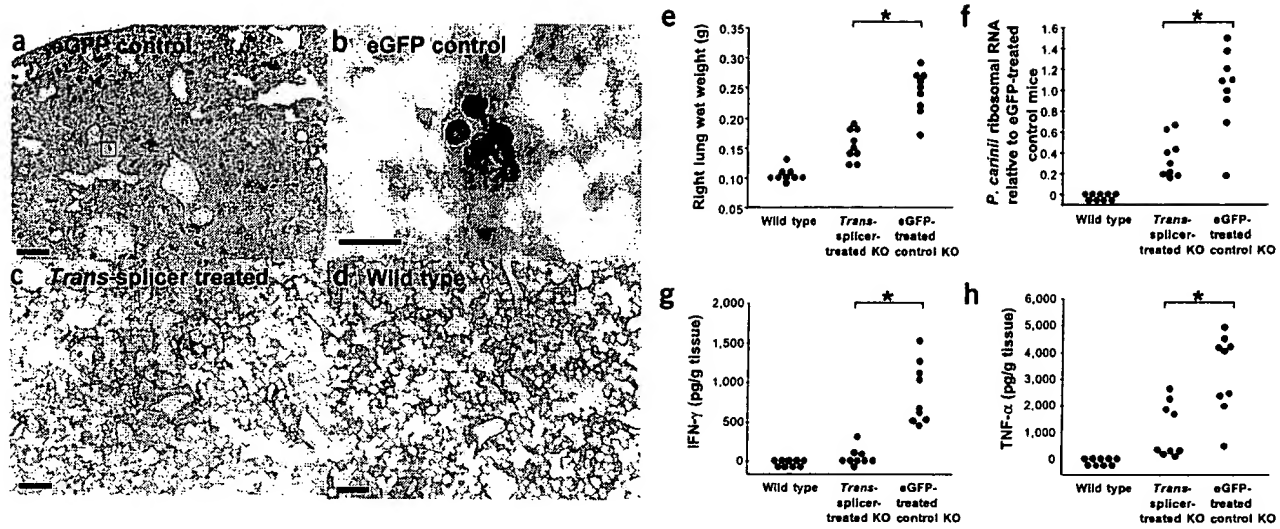

Figure 5 *Trans*-spliced, CD40L-mediated attenuation of *P. carinii* infection in CD40L-knockout mice. (a–d) Lung histology 8 weeks after *P. carinii* infection of *trans*-splicer-treated CD40L-knockout mice. Representative GMS stains of the lungs of wild-type, *trans*-splicer-treated CD40L-knockout and LVeGFP-treated CD40L-knockout mice after intratracheal challenge with 2×10^6 *P. carinii*. (a) Low-magnification lung section from an LVeGFP-treated CD40L-knockout mouse infected with *P. carinii*. Box indicates the area magnified in b. (b) Same as a, high magnification. (c) Low-magnification lung section from a *trans*-splicer-treated CD40L-knockout mouse infected with *P. carinii*. (d) Low-magnification lung section from a wild-type mouse infected with *P. carinii*. Bar, 100 μm (a,c,d), 10 μm (b). (e) *Trans*-spliced CD40L-mediated decrease in wet weight of right lung from mice infected with *P. carinii*. (f) Quantitation of *P. carinii* ribosomal RNA per right lung of infected mice using real-time quantitative RT-PCR. The mean of *P. carinii* ribosomal RNAs of LVeGFP-treated knockout mice was set at 1. In both panels, each circle represents one mouse. (g) Impact of *trans*-spliced CD40L on IFN-g levels. (h) Impact on TNF-a levels. IFN-g and TNF-a were assessed by ELISA in lung homogenates of mice infected with *P. carinii* as described above. For both panels, each circle represents one mouse. $^*P < 0.005$, *trans*-splicer-treated knockout mice versus LVeGFP-treated knockout mice.

in lung homogenate relative to LVeGFP-treated mice (mean, 1,066 pg/g tissue and 3,231 pg/g tissue respectively; $P < 0.005$ *trans*-splicer treated knockout versus eGFP-treated control knockout; Fig. 5h).

CD40L correction does not lead to lymphoproliferative disease

The lymphoproliferative disease developing by 6–9 months after therapy observed in prior studies of retroviral-mediated constitutive expression of normal CD40L cDNA in CD40L-knockout mice[13] suggested that natural regulation of CD40L is essential to the development of gene delivery as a therapy. To assess the possible development of lymphoproliferative disease in the *trans*-spliced CD40L transplant recipients, mice were inspected for gross anatomical pathology, and thymus, spleen and inguinal lymph nodes from mice were examined histologically. By 12 months after transplantation, none of 26 mice evaluated had developed either gross or microscopic lymphoproliferative disease, representing a very low risk of such disease as compared with two previous studies ($P < 0.0002$). There was a significant difference in incidence rates ($P < 0.0001$) and further analysis using pairwise multiple comparisons between each pair of studies showed that the incidence rates for the studies of Brown *et al.*[13] and Sacco *et al.*[14] were significantly greater than for our study (63%, 33%, 0%; $P < 0.0001$ (Brown's study versus our study) and $P < 0.0002$ (Sacco's study versus our study), respectively). As the result is highly significant, the issue of a type II error (beta error) is moot. Accordingly, it is not necessary to perform a sample size and power calculation. These results suggest that regulated expression of CD40L is required to avoid the development of lymphoproliferative disease, and that regulated *trans*-spliced CD40L delivered by means of lentiviral vectors and bone marrow transplantation may be a safe therapeutic approach to HIGM1.

DISCUSSION

We have used lentivirus-mediated *trans*-splicing to correct a mouse model of HIGM1 syndrome, preserving the naturally controlled endogenous levels of CD40L mRNA. We demonstrate that by optimizing the sequence, size and location of the hybridization domain of the exogenous *trans*-splicer, the correct 3′ region of the CD40L mRNA can be spliced into the normal 5′ portion of the endogenous RNA using gene transfer to bone marrow cells to correct a mouse CD40L-knockout model of HIGM1. After transplantation of the corrected cells to naive CD40L-knockout mice, the recipients demonstrated antigen-specific IgG1 responses to KLH, regulated expression of CD40L on stimulated $CD4^+$ T cells in primary and secondary transplanted mice, and marked attenuation of proliferation of *P. carinii* in the lung after respiratory tract challenge. Assessment of the lentivirus-mediated, CD40L-corrected CD40L-knockout mice up to 1 year showed no evidence of lymphoproliferative disease. Thus, it is possible to correct the HIGM1 syndrome by *trans*-splicing correction at the mRNA leading to functional correction of the gene mutation while preserving the regulation of the critically important, powerful CD40L gene.

Lentivirus-mediated transfer of the normal 3′ coding sequences of the CD40L gene to CD40L-knockout mice demonstrated persistent correction for at least 10 weeks (the longest time assessed), and secondary transplanted mice demonstrated similar levels of correction. Previous studies by Liu *et al.*[18] have shown that an adenovirus gene transfer vector coding for a 3′ *trans*-splicer can be used to correct a human airway epithelium explant model for a mutation in the cystic fibrosis transmembrane regulator gene, and Chao *et al.*[21] have demonstrated an adenovirus-delivered 3′ *trans*-splicer to transiently correct a mouse model of factor VIII hemophilia. Our study extends

the use of *trans*-splicing to engraft hematopoietic stem cells with persistent, functional correction of a genetic defect.

For many gene therapy applications it is satisfactory to use a constitutive promoter to drive the transgene. However, in applications where constitutive expression of the gene product can be deleterious, it is critical to regulate the expression of the exogenous transgene. There are several ways to accomplish this. If the appropriate regulatory sequences for the gene of interest are known, they can be built into the expression cassette[29]. By splicing into the endogenous mRNA, *trans*-splicing leverages the endogenous regulatory processes that control mRNA levels, thus circumventing the need to define the regulatory elements. As long as the proportion of endogenous mRNA that is corrected remains the same, independent of the level of gene expression, *trans*-splicing correction should parallel the endogenous control mechanisms. In our study, this seems to be the case, with CD3 triggering of CD40L expression increasing and then decreasing as in the normal regulatory process of $CD4^+$ T-cell activation. Whereas constitutive expression of CD40L results in lymphoproliferative disease[13,14], none was observed in the corrected CD40L-knockout mice observed over a period of 1 year in our study.

Brown and colleagues[13] reported that retrovirus-mediated transfer by means of bone marrow of the full-length CD40L cDNA transfer to CD40L-knockout mice resulted in successful restoration of cellular and humoral immunity, but 12 of 19 treated mice developed T-lymphoproliferative disorders 6–9 months after treatment. These investigators concluded that insertional mutagenesis did not contribute to development of the lymphomas, as only a minor proportion of tumor cells contained proviral DNA, and the level of proviral DNA was no higher than the proviral DNA level of non-tumor transplanted bone marrow cells. Similarly, Sacco and colleagues[14] observed that CD40L-transgenic mice without regulated expression of CD40L resulted in 35 of 105 mice developing atypical lymphoid proliferation, which occasionally progressed to frank lymphomas at ages from 6 to 12 months. The Sacco *et al.*[14] study used HTLV1 promoters, and the investigators concluded that gene transfer of constitutively expressed genes for hereditary defects involving genes implicated in cell proliferation, which were normally under strict regulation, could be dangerous.

Like individuals with HIGM1 syndrome, CD40L-knockout mice are highly susceptible to opportunistic infection, including *P. carinii*, *Candida*, *Schistosoma mansoni*, *Cryptosporidium parvum*, lymphocytic choriomeningitis virus and *Leishmania*[30–36]. Several lines of evidence in our study demonstrated that CD40L *trans*-splicing correction of the CD40L-knockout mice substantially enhanced the ability of these immunodeficient mice to attenuate a respiratory tract challenge with *P. carinii*. Previous studies have shown that chronic *P. carinii* pneumonia results in a decrease of body weight in CD40L-knockout mice and an increase in expression of IFN-γ and TNF-α in the lungs of mice depleted for $CD4^+$ T cells[27,28,30]. Attenuation of these parameters was observed in lungs of *trans*-splicer-treated CD40L-knockout mice, suggesting that *trans*-spliced CD40L ameliorates chronic *P. carinii* pneumonia in this model. In addition, histological and quantitative analysis confirmed that the presence of *trans*-spliced CD40L correlates with the attenuation of *P. carinii* pneumonia.

In addition to targeting HIGM1 in an animal model, other genetic repair strategies have shown promise in primary human cells (for example, erythrocyte precursors taken from patients with sickle cell disease or β-thalassemia) or in animal models of human disease (for example, cystic fibrosis or hemophilia)[15]. Current efforts are focused largely on making these repairs efficient enough for clinical therapeutic benefit[15]. In this study, low efficiency of transduction of vector to target cells and low efficiency of *trans*-splicing resulted in partial phenotypic correction in mice. Low efficiency would be a major potential limitation for the application of *trans*-splicing to human disease. Fortunately, in our study, transduced cells expressing CD40L allowed target cells to be amplified, ultimately generating an alteration in the disease phenotype. However, this situation will only exist in a small number of genetic diseases. Improving the efficiency of *trans*-splicing will render more diseases approachable by this technique.

METHODS

Protection against *P. carinii*. Animals were maintained and treated in accordance with the Institutional Animal Care and Use Committee of Weill Medical College of Cornell University and the US National Institutes of Health *Guide for the Care and Use of Laboratory Animals*. To assess the immune responses to a live pathogen relevant to HIGM1 disease, *P. carinii* organisms were isolated from lungs of BALB/c nude mice (Taconic Labs) previously inoculated with *P. carinii*[37]. *P. carinii* were purified by centrifugation, and protein antigen for ELISA was produced by sonication for 5 min as described[38]. Briefly, frozen lungs were homogenized in 10 ml homogenization buffer (58.5 mM disodium phosphate, 1.5 mM monopotassium phosphate, 43.5 mM sodium chloride, 10 mM trisodium citrate, 10 mM dithiothreitol and 2.7 mM potassium chloride, pH 7.4), in a tissue grinder (Dounce; Wheaton), filtered through sterile gauze and centrifuged at 32*g* for 5 min to remove large debris. The supernatant was centrifuged at 5,000*g* for 10 min, and the pellet was resuspended in homogenization buffer and stained with modified Giemsa stain (Diff-Quik; Baxter). *P. carinii* was quantified microscopically[37], and the inoculum concentration was adjusted to 4×10^7 *P. carinii* organisms per ml. Gram stains were performed on the inoculum to exclude contamination with bacteria.

C57BL/6 wild-type, *trans*-splicer-treated CD40L-knockout and control eGFP-treated CD40L-knockout mice were infected intratracheally with 2×10^6 *P. carinii* organisms in 50 μl PBS. Wild-type control mice were injected intratracheally with 50 μl PBS. At 8 weeks after infection, mice were sacrificed and body weight was measured. Lungs and sera were collected, and left lungs were fixed with 4% paraformaldehyde for 8 h and embedded in paraffin. Lung sections were stained with H&E or GMS to detect *P. carinii*[38]. After right lung weight was measured, RNA was isolated for assessment of *P. carinii* ribosomal RNA levels. Real-time quantitative RT-PCR against *P. carinii* ribosomal RNA was used to assess levels of *P. carinii* infection in the lung using PCR primers 5′-ATGAGGTGAAAAGTCGAAAGGG-3′ and 5′-TGAGGTCTCAGATGAAAAACCTCTT-3′[38]. The probe labeled with 6FAM had the sequence 5′-6FAM-AACAGCCCAGAATAATGAATAAAGTTCCTCAATTGTTACTAMRA-3′[38]. Real-time PCR was done as described above, and *P. carinii* ribosomal RNA was calculated relative to an eGFP-treated control. Right lungs were also used to determine IFN-γ and TNF-α protein levels. The right lung specimens were homogenized in 10% (w/v) lung homogenate buffer (150 mM sodium chloride, 1 mM calcium chloride, 1 mM magnesium chloride, 0.5% Triton X-100, 15 mM Tris-HCl, pH 7.4) and centrifuged at 2,000*g* for 10 min to remove debris. The supernatant was collected and IFN-γ and TNF-α were evaluated by ELISA (R&D Systems). To assess *P. carinii*–specific IgM and IgG1, *P. carinii*–specific ELISA was carried out with 96-well plates coated with *P. carinii* protein antigen (1 μg/well) as described above.

Assessment of lymphoproliferative disease. To assess whether the CD40L-corrected *trans*-spliced CD40L-knockout mice developed lymphoproliferative disease, mice were sacrificed 3–12 months after transplantation and inspected for gross anatomical pathology. Thymus, spleen and inguinal lymph nodes were collected and embedded in paraffin. Tissue sections were stained with H&E to analyze for the presence of lymphoproliferative disease.

Statistical analysis. Comparisons for *in vitro* experiments were made using the two-tailed Student's *t*-test and comparisons for *in vivo* experiments were made by Mann-Whitney's U-test. Comparisons for risk of development of lymphoproliferative disease were made by Fisher's exact probability test among the previous two results and our result. The Fisher exact test was used to compare the 12-month incidence rates of lymphoproliferative disease across the three studies. Normally, one would perform a more formal 'survival analysis' on such data (where time would be 'time until development of lymphoprolifera-

tive disease'). Given that the raw data for the two published studies were not available, we chose to pick a common point in time, such that lymphoproliferative disease status was known on all mice at that time. The chosen time was 12 months, as our study (C) followed all mice for at least 12 months and each mouse's status was known at 12 months. As for the other 2 studies, Brown's study (A) reported incidence rates at 6–9 months of follow up and Sacco's study (B) at 6–12 months. Even though the status of a mouse only followed for, say, 6 months was not definitively known at 12 months, the published incidence rates serve as lower bounds for the actual 12-month rates in A and B. Therefore, the actual 12-month rates would be at least as great compared with C, thus yielding even more significant results.

Further information. The design and construction of *trans*-splicer expression cassettes[39], the optimization of *trans*-splicer hybridization domains[39], the *in vitro* assessment of CD40L protein produced by *trans*-splicing[40], the functional analysis of *trans*-spliced CD40L *in vitro*[41], the packaging and infection of lentiviral vectors[42–44], the *ex vivo* lentivirus-mediated gene transfer to bone marrow cells[45], the secondary transplantation, the real-time quantitative PCR and RT-PCR *in vivo*, the restoration of immunity against a thymus-dependent antigen and the assessment of regulated expression of CD40L (refs. 46–48) were done according to standard methodology. Details are given in the Supplementary Methods online.

Supplementary information is available on the Nature Medicine website.

ACKNOWLEDGMENTS

We thank K. Nakayama and Q. Jiang for help in construction of *trans*-splicing vectors; A. Busch for flow cytometry analysis; N. Hackett and A. Ciecuich for real-time RT-PCR analysis; K. Kasuya for histological analysis; T. Kafri for providing plasmid; and N. Mohamed for help preparing this manuscript. These studies were supported, in part, by U01 HL66952, the Will Rogers Memorial Fund and The Malcolm Hewitt Wiener Foundation.

COMPETING INTERESTS STATEMENT

The authors declare that they have no competing financial interests.

Received 22 January; accepted 29 June 2004
Published online at http://www.nature.com/naturemedicine/

1. Callard, R.E., Armitage, R.J., Fanslow, W.C. & Spriggs, M.K. CD40 ligand and its role in X-linked hyper-IgM syndrome. *Immunol. Today* **14**, 559–564 (1993).
2. Kroczek, R.A. *et al.* Defective expression of CD40 ligand on T cells causes "X-linked immunodeficiency with hyper-IgM (HIGM1)". *Immunol. Rev.* **138**, 39–59 (1994).
3. Di Santo, J.P., Bonnefoy, J.Y., Gauchat, J.F., Fischer, A. & de Saint, B.G. CD40 ligand mutations in X-linked immunodeficiency with hyper-IgM. *Nature* **361**, 541–543 (1993).
4. Korthauer, U. *et al.* Defective expression of T-cell CD40 ligand causes X-linked immunodeficiency with hyper-IgM. *Nature* **361**, 539–541 (1993).
5. Roy, M., Waldschmidt, T., Aruffo, A., Ledbetter, J.A. & Noelle, R.J. The regulation of the expression of gp39, the CD40 ligand, on normal and cloned CD4+ T cells. *J. Immunol.* **151**, 2497–2510 (1993).
6. Stout, R.D., Suttles, J., Xu, J., Grewal, I.S. & Flavell, R.A. Impaired T cell-mediated macrophage activation in CD40 ligand-deficient mice. *J. Immunol.* **156**, 8–11 (1996).
7. Grewal, I.S. & Flavell, R.A. CD40 and CD154 in cell-mediated immunity. *Annu. Rev. Immunol.* **16**, 111–135 (1998).
8. Straw, A.D., MacDonald, A.S., Denkers, E.Y. & Pearce, E.J. CD154 plays a central role in regulating dendritic cell activation during infections that induce Th1 or Th2 responses. *J. Immunol.* **170**, 727–734 (2003).
9. Gennery, A.R. *et al.* Treatment of CD40 ligand deficiency by hematopoietic stem cell transplantation: a survey of the European experience, 1993-2002. *Blood* **103**, 1152–1157 (2004).
10. Levy, J. *et al.* Clinical spectrum of X-linked hyper-IgM syndrome. *J. Pediatr.* **131**, 47–54 (1997).
11. Hadzic, N. *et al.* Correction of the hyper-IgM syndrome after liver and bone marrow transplantation. *N. Engl. J. Med.* **342**, 320–324 (2000).
12. Thomas, C. *et al.* Brief report: correction of X-linked hyper-IgM syndrome by allogeneic bone marrow transplantation. *N. Engl. J. Med.* **333**, 426–429 (1995).
13. Brown, M.P. *et al.* Thymic lymphoproliferative disease after successful correction of CD40 ligand deficiency by gene transfer in mice. *Nat. Med.* **4**, 1253–1260 (1998).
14. Sacco, M.G. *et al.* Lymphoid abnormalities in CD40 ligand transgenic mice suggest the need for tight regulation in gene therapy approaches to hyper immunoglobulin M (IgM) syndrome. *Cancer Gene Ther.* **7**, 1299–1306 (2000).
15. Sullenger, B.A. Targeted genetic repair: an emerging approach to genetic therapy. *J. Clin. Invest.* **112**, 310–311 (2003).
16. Puttaraju, M., Jamison, S.F., Mansfield, S.G., Garcia-Blanco, M.A. & Mitchell, L.G. Spliceosome-mediated RNA *trans*-splicing as a tool for gene therapy. *Nat. Biotechnol.* **17**, 246–252 (1999).
17. Garcia-Blanco, M.A., Puttaraju, M., Mansfield, S.G. & Mitchell, L.G. Spliceosome-mediated RNA *trans*-splicing in gene therapy and genomics. *Gene Ther. Regul.* **1**, 141–163 (2000).
18. Liu, X. *et al.* Partial correction of endogenous DeltaF508 CFTR in human cystic fibrosis airway epithelia by spliceosome-mediated RNA *trans*-splicing. *Nat. Biotechnol.* **20**, 47–52 (2002).
19. Mansfield, S.G. *et al.* Repair of CFTR mRNA by spliceosome-mediated RNA *trans*-splicing. *Gene Ther.* **7**, 1885–1895 (2000).
20. Puttaraju, M., Di Pasquale, J., Baker, C.C., Mitchell, L.G. & Garcia-Blanco, M.A. Messenger RNA repair and restoration of protein function by spliceosome-mediated RNA *trans*-splicing. *Mol. Ther.* **4**, 105–114 (2001).
21. Chao, H. *et al.* Phenotype correction of hemophilia A mice by spliceosome-mediated RNA *trans*-splicing. *Nat. Med.* **9**, 1015–1019 (2003).
22. Garcia-Blanco, M.A. Messenger RNA reprogramming by spliceosome-mediated RNA *trans*-splicing. *J. Clin. Invest.* **112**, 474–480 (2003).
23. Bonen, L. *Trans*-splicing of pre-mRNA in plants, animals, and protists. *FASEB J.* **7**, 40–46 (1993).
24. Caudevilla, C. *et al.* Natural *trans*-splicing in carnitine octanoyltransferase pre-mRNAs in rat liver. *Proc. Natl. Acad. Sci. USA* **95**, 12185–12190 (1998).
25. Xu, J. *et al.* Mice deficient for the CD40 ligand. *Immunity.* **1**, 423–431 (1994).
26. Testi, R., D'Ambrosio, D., De Maria, R. & Santoni, A. The CD69 receptor: a multipurpose cell-surface trigger for hematopoietic cells. *Immunol. Today* **15**, 479–483 (1994).
27. Kolls, J.K., Beck, J.M., Nelson, S., Summer, W.R. & Shellito, J. Alveolar macrophage release of tumor necrosis factor during murine *Pneumocystis carinii* pneumonia. *Am. J. Respir. Cell Mol. Biol.* **8**, 370–376 (1993).
28. Kolls, J.K. *et al.* IFN-γ and CD8+ T cells restore host defenses against *Pneumocystis carinii* in mice depleted of CD4+ T cells. *J. Immunol.* **162**, 2890–2894 (1999).
29. Logan, A.C., Lutzko, C. & Kohn, D.B. Advances in lentiviral vector design for gene-modification of hematopoietic stem cells. *Curr. Opin. Biotechnol.* **13**, 429–436 (2002).
30. Baumgartner, R. *et al.* Evidence for the requirement of T cell costimulation in the pathogenesis of natural *Pneumocystis carinii* pulmonary infection. *Microb. Pathog.* **33**, 193–201 (2002).
31. Campbell, K.A. *et al.* CD40 ligand is required for protective cell-mediated immunity to *Leishmania major*. *Immunity* **4**, 283–289 (1996).
32. MacDonald, A.S. *et al.* Impaired Th2 development and increased mortality during *Schistosoma mansoni* infection in the absence of CD40/CD154 interaction. *J. Immunol.* **168**, 4643–4649 (2002).
33. Netea, M.G., Meer, J.W., Verschueren, I. & Kullberg, B.J. CD40/CD40 ligand interactions in the host defense against disseminated *Candida albicans* infection: the role of macrophage-derived nitric oxide. *Eur. J. Immunol.* **32**, 1455–1463 (2002).
34. Soong, L. *et al.* Disruption of CD40-CD40 ligand interactions results in an enhanced susceptibility to *Leishmania amazonensis* infection. *Immunity* **4**, 263–273 (1996).
35. Stephens, J., Cosyns, M., Jones, M. & Hayward, A. Liver and bile duct pathology following *Cryptosporidium parvum* infection of immunodeficient mice. *Hepatology* **30**, 27–35 (1999).
36. Thomsen, A.R., Nansen, A., Christensen, J.P., Andreasen, S.O. & Marker, O. CD40 ligand is pivotal to efficient control of virus replication in mice infected with lymphocytic choriomeningitis virus. *J. Immunol.* **161**, 4583–4590 (1998).
37. Merali, S., Chin, K., Grady, R.W., Weissberger, L. & Clarkson, A.B. Response of rat model of *Pneumocystis carinii* pneumonia to continuous infusion of deferoxamine. *Antimicrob. Agents Chemother.* **39**, 1442–1444 (1995).
38. Zheng, M. *et al.* CD4+ T cell-independent vaccination against *Pneumocystis carinii* in mice. *J. Clin. Invest.* **108**, 1469–1474 (2001).
39. Pergolizzi, R.G. *et al. In vivo trans*-splicing of 5′ and 3′ segments of pre-mRNA directed by corresponding DNA sequences delivered by gene transfer. *Mol. Ther.* **8**, 999–1008 (2003).
40. Armitage, R.J. *et al.* Molecular and biological characterization of a murine ligand for CD40. *Nature* **357**, 80–82 (1992).
41. Field, J. *et al.* Purification of a RAS-responsive adenylyl cyclase complex from *Saccharomyces cerevisiae* by use of an epitope addition method. *Mol. Cell. Biol.* **8**, 2159–2165 (1988).
42. Xu, K., Ma, H., McCown, T.J., Verma, I.M. & Kafri, T. Generation of a stable cell line producing high-titer self-inactivating lentiviral vectors. *Mol. Ther.* **3**, 97–104 (2001).
43. Naldini, L. *et al. In vivo* gene delivery and stable transduction of nondividing cells by a lentiviral vector. *Science* **272**, 263–267 (1996).
44. Dull, T. *et al.* A third-generation lentivirus vector with a conditional packaging system. *J. Virol.* **72**, 8463–8471 (1998).
45. Szilvassy, S.J., Lansdorp, P.M., Humphries, R.K., Eaves, A.C. & Eaves, C.J. Isolation in a single step of a highly enriched murine hematopoietic stem cell population with competitive long-term repopulating ability. *Blood* **74**, 930–939 (1989).
46. Vigna, E. *et al.* Robust and efficient regulation of transgene expression *in vivo* by improved tetracycline-dependent lentiviral vectors. *Mol. Ther.* **5**, 252–261 (2002).
47. Follenzi, A., Ailles, L.E., Bakovic, S., Geuna, M. & Naldini, L. Gene transfer by lentiviral vectors is limited by nuclear translocation and rescued by HIV-1 pol sequences. *Nat. Genet.* **25**, 217–222 (2000).
48. Kikuchi, T., Worgall, S., Singh, R., Moore, M.A. & Crystal, R.G. Dendritic cells genetically modified to express CD40 ligand and pulsed with antigen can initiate antigen-specific humoral immunity independent of CD4+ T cells. *Nat. Med.* **6**, 1154–1159 (2000).

Partial correction of endogenous ΔF508 CFTR in human cystic fibrosis airway epithelia by spliceosome-mediated RNA *trans*-splicing

Xiaoming Liu[1†], Qinshi Jiang[1†], S. Gary Mansfield[4], M. Puttaraju[4], Yulong Zhang[1,3], Weihong Zhou[1], Jonathan A. Cohn[5], Mariano A. Garcia-Blanco[4], Lloyd G. Mitchell[4], and John F. Engelhardt[1-3*]

Spliceosome-mediated RNA *trans*-splicing (SMaRT) was investigated as a means for functionally correcting endogenous ΔF508 cystic fibrosis transmembrane conductance regulator (CFTR) transcripts using *in vitro* human cystic fibrosis (CF) polarized airway epithelia and *in vivo* human CF bronchial xenografts. Recombinant adenovirus (Ad.*CFTR*-PTM) encoding a pre-therapeutic molecule (PTM) targeted to CFTR intron 9 corrected transepithelial cyclic AMP (cAMP)-sensitive short-circuit current (Isc) in ΔF508 homozygous epithelia to a level 16% of that observed in normal human bronchial epithelia. Molecular analyses using RT-PCR and western blotting confirmed SMaRT-mediated partial correction of endogenous ΔF508 messenger RNA (mRNA) transcripts and protein. In an *in vivo* model of ΔF508 CF airway epithelia, human CF bronchial xenografts infected with Ad.*CFTR*-PTM also demonstrated partial correction of CFTR-mediated Cl^- permeability at a level 22% of that seen in non-CF xenografts. These results provide functional evidence for SMaRT-mediated repair of mutant endogenous CFTR mRNA in intact polarized CF airway epithelial models.

Since the cloning of the *CFTR* gene in 1989, numerous studies have attempted to develop safe and effective methods for correcting the *CFTR* gene defect in the lungs of CF patients. The majority of studies in this area have focused on identifying appropriate gene-delivery systems to the lung[1,2]. However, a potential hurdle in gene-addition approaches is the need to regulate CFTR expression in the appropriate cell types in the airway. Superimposed on the functional complexities of CFTR as a chloride channel and regulator of other channels is its diverse and heterogeneous expression profile in various airway cell types[3]. CFTR is expressed at high levels in a subset of cells in the surface airway epithelium and submucosal glands and at lower levels in ciliated cells[3]. Thus, high levels of ectopic CFTR expression in CF airway epithelia may inadequately complement the pathophysiological processes that lead to chronic bacterial infection in the CF lung. Researchers have attempted to define regulatory elements required for appropriate expression of recombinant CFTR in the airway[4], but strategies that require large regulatory elements are often limited by vector packaging capacity. Hence, repair of the defective CFTR gene product has theoretical and practical advantages for restoring physiological CFTR function.

Cis-splicing of pre-mRNA to mRNA is essential for gene expression. Splicing is catalyzed by a complex called the spliceosome[5]. An uncommon and less characterized mechanism for RNA processing involves *trans*-splicing between different pre-mRNA molecules; this process has been demonstrated to form functional hybrid mRNAs in a number of mammalian systems[6,7]. Recently, a technology to reprogram pre-mRNA by spliceosome-mediated RNA *trans*-splicing (SMaRT) was developed[8-10]. Using SMaRT, Mansfield *et al.* successfully corrected mutations in cells expressing a ΔF508 *CFTR* mini-gene[8]. However, the ability to correct endogenous mutant CFTR was not tested. In the present study, we have demonstrated that SMaRT can correct endogenous ΔF508 mutant CFTR pre-mRNA in CF airway epithelia and partially restore CFTR-mediated chloride transport.

Results

Partial correction of CFTR Cl^- conductance in ΔF508 CF airway epithelia *in vitro*. We demonstrated earlier that PTMs carrying exons 10–24 of CFTR can repair mRNA derived from a ΔF508-*CFTR* mini-gene by SMaRT (ref. 8). To investigate whether SMaRT could efficiently correct endogenous ΔF508 CFTR transcripts in polarized human CF airway epithelia, we generated two adenoviral constructs encoding two different CFTR PTMs (Fig. 1). Infection of CF airway cultures with either Ad.*CFTR*PTM-15 or Ad.*CFTR*PTM-24 (multiplicity of infection (MOI) = 2,000 particles/cell) provided significant complementation (12–16%) of 3-isobutyl-1-methylxanthine (IBMX)/ forskolin-inducible Isc_{max} as compared with non-CF controls (Fig. 2). Following amiloride inhibition of epithelial sodium conductance, increases in CFTR transepithelial Cl^- current were observed in response to IBMX/forskolin stimulation. Addition of bumetanide, which blocks uptake of Cl^- from the basolateral membrane, inhibited IBMX/forskolin-stimulated Isc and indicated that changes in Cl^- movement were due to active transport and not passive diffusion (Fig. 2B). Correction with Ad.*CFTR*PTM-24 and Ad.*CFTR*PTM-15 was approximately equivalent to that achieved with a recombinant adenovirus encoding full-length CFTR complementary DNA (cDNA) (Ad.CMV*CFTR*)[11] at an MOI 10-fold lower than that used for the PTM constructs (MOI = 200 particles/cell). No functional correction with Ad.*CFTR*PTM-15 or Ad.*CFTR*PTM-24

*Departments of [1]Anatomy and Cell Biology and [2]Internal Medicine, and [3]The Center for Gene Therapy of Cystic Fibrosis and Other Genetic Diseases, College of Medicine, The University of Iowa, Iowa City, IA 52242. [4]Intronn Inc, Raleigh, NC 27606. [5]Department of Medicine, Duke University Medical Center, Durham, NC 27710. *Corresponding author (john-engelhardt@uiowa.edu). [†]These authors contributed equally to this work.*

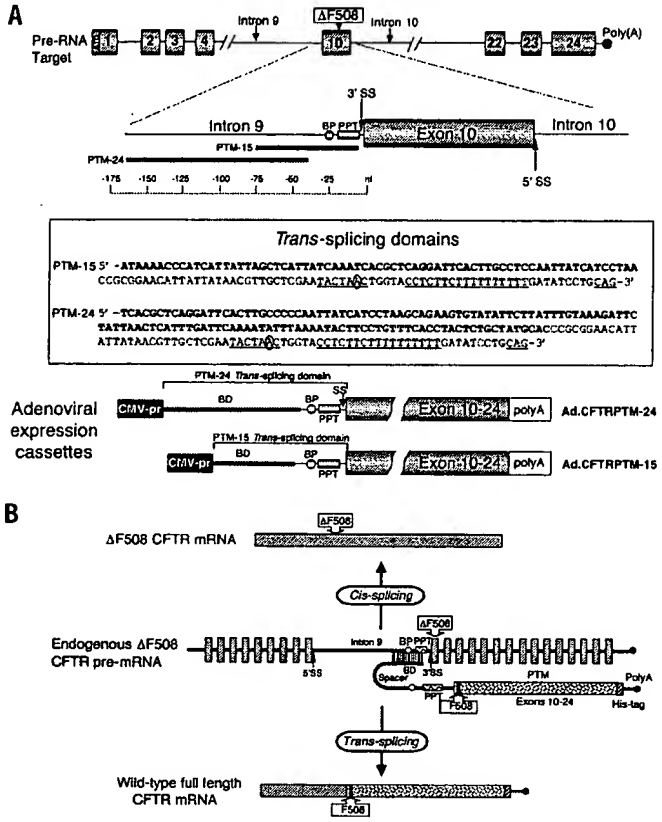

Figure 1. Schematic diagrams of CFTR PTMs and pre-mRNA target. (A) PTM-15 and PTM-24 differ only in their binding domain sequences, defined as the length and regions of base pairing to CFTR intron 9. The complete sequence of each PTM *trans*-splicing domain (TSD) is shown in the boxed region. For each TSD, the PTM binding domain sequence is printed in bold and the splice elements (BP, PPT, and splice acceptor site) are underlined. The presumed BP adenosine used in lariat formation is circled. The structures of PTM-15 and PTM-24 *trans*-splicing cassettes cloned within recombinant adenoviral vectors are shown below. (B) Schematic representation of the SMaRT mechanism. BD, Binding domain; BP, branchpoint; PPT, polypyrimidine tract; SS, splice site.

was seen at MOIs of 200 particles/cell (data not shown). Importantly, CF epithelia infected with a negative control adenovirus (Ad.LacZPTM-24) carrying a 3'-segment of LacZ[9,12] (Fig. 2C) produced no IBMX/forskolin responses and also controlled for the integrity of the epithelium following adenoviral infection. A summary of data obtained from multiple experiments is shown in Figure 2D. Infection with Ad.*CFTR*PTM-15 and Ad.*CFTR*PTM-24 elicited IBMX/forskolin-induced changes in Isc that were 11.9% and 16.0% of the level in normal human airway cells, respectively. In contrast, infection with the control (Ad.LacZPTM-24) resulted in a slight decrease in Isc following IBMX/forskolin treatment.

Detection of *trans*-spliced CFTR mRNA and protein. SMaRT repair was evaluated by the presence of the F508 codon in CFTR mRNA derived from polarized epithelia infected with Ad.*CFTR*PTM-24. RT-PCR products generated with allele-specific primers were evaluated by gel electrophoresis and allele-specific oligonucleotide hybridization. PCR analysis of plasmid controls demonstrated the specificity of these assays (Fig. 3, lanes 10–13). ΔF508-specific RT-PCR products were detected in all primary CF airway cultures tested (Fig. 3, lanes 1–3). No products were detected when reverse transcriptase was omitted, demonstrating specificity for mRNA (lanes 4 and 8). Wild-type F508-specific RT-PCR products were not detected in ΔF508 human airway cells infected with a control adenovirus (lane 7) but were produced in airway cultures infected with Ad.*CFTR*PTM-24 (lane 5) or full-length Ad.CMV*CFTR* (lane 6). These results confirmed the correction of ΔF508 CFTR transcripts in our primary culture model. Allele-specific oligonucleotide hybridization was performed to exclude the possibility of nonspecific amplification (Fig. 3). These experiments confirmed that the wild-type F508 CFTR codon was present only in samples infected with Ad.*CFTR*PTM-24 or Ad.CMV*CFTR*.

To assess whether cells infected with Ad.*CFTR*PTM-24 were capable of producing fully processed CFTR protein, we evaluated CFTR protein levels using two immunoprecipitation approaches. Unfortunately, the amount of material harvested from non-CF polarized airway cultures was insufficient to detect wild-type *CFTR*. Thus, alternative systems were used to confirm the ability of Ad.*CFTR*PTM-24 to correct ΔF508 CFTR protein. The first model tested for corrected protein in HeLa cells expressing a CFTR mini-gene target[8]. CFTR was immunoprecipitated using a polyclonal anti-CFTR antibody followed by western blotting with an N-terminal specific anti-CFTR antibody. These studies confirmed that pre-mRNA from a *CFTR* mini-gene target could be corrected to produce CFTR protein following Ad.*CFTR*PTM-24 infection (Fig. 4A, lane 1). The banding pattern and size of the immunoreactive protein products were similar to those seen following expression of full-length CFTR protein with the Ad.CMV*CFTR* control (lane 2). No immunoreactive CFTR protein was detected in controls transfected with Ad.*CFTR*PTM-24 or mini-gene target alone (lanes 3 and 4). Estimates of the level of correction with Ad.*CFTR*PTM-24 were ~2% of that seen at equivalent MOIs with Ad.CMV*CFTR*, assuming 100% recovery by immunoprecipitation. Although these data demonstrate that Ad.*CFTR*PTM-24 is functional, they do not address endogenous CFTR mRNA repair. To this end, we evaluated *trans*-splicing in T84 cells that produce high levels of CFTR protein. As this cell line harbors the normal F508 sequence, the His-tag incorporated into the C terminus of CFTR was used as a marker for *trans*-splicing and protein correction.

Trans-spliced CFTR protein expressed in T84 cells was affinity-captured with Ni-NTA magnetic agarose beads and detected by western blotting with an anti-N-terminal CFTR antibody. As shown in Figure 4B, CFTR immunoreactivity detected in Ad.*CFTR*PTM-24–infected T84 cells (lane 2) demonstrated a banding pattern comparable to that of the fully processed wild-type CFTR (lane 3). Importantly, CFTR immunoreactivity was absent in T84 cells that were not infected with Ad.*CFTR*PTM-24 (lane 1). The efficiency of adenoviral infection of T84 cells was ~20% according to green fluorescent protein (GFP) reporter gene expression. Based on this infection efficiency and the abundance of His-tagged CFTR (Fig. 4B, lane 2 vs. lane 3), the level of full-length CFTR immunoreactivity following Ad.*CFTR*PTM-24 infection was ~0.2% that of the endogenous protein. However, the efficiency of Ni-NTA precipitation is currently unknown, making such calculations nonquantitative. Nonetheless, these results demonstrate that delivery of Ad.*CFTR*PTM-24 into CFTR-expressing cells can generate *trans*-spliced, full-length, CFTR protein.

In vivo correction of CFTR Cl^- permeability in ΔF508 CF bronchial xenografts. To further evaluate the functional correction of CFTR by SMaRT in a more native model of the human airway, we used an *in vivo* human bronchial xenograft model system[13,14]. ΔF508 homozygous CF xenografts were infected twice with Ad.*CFTR*PTM-24 or Ad.*LacZ*PTM24 control virus. Serial infection typically gives ~50% transduction of airway epithelia[14]. Infected xenografts were analyzed for cAMP-inducible changes in CFTR-mediated Cl^- permeability by monitoring transepithelial potential difference (PD)[13]. As summarized in Figure 5, cAMP/forskolin-induced changes in PD were significantly

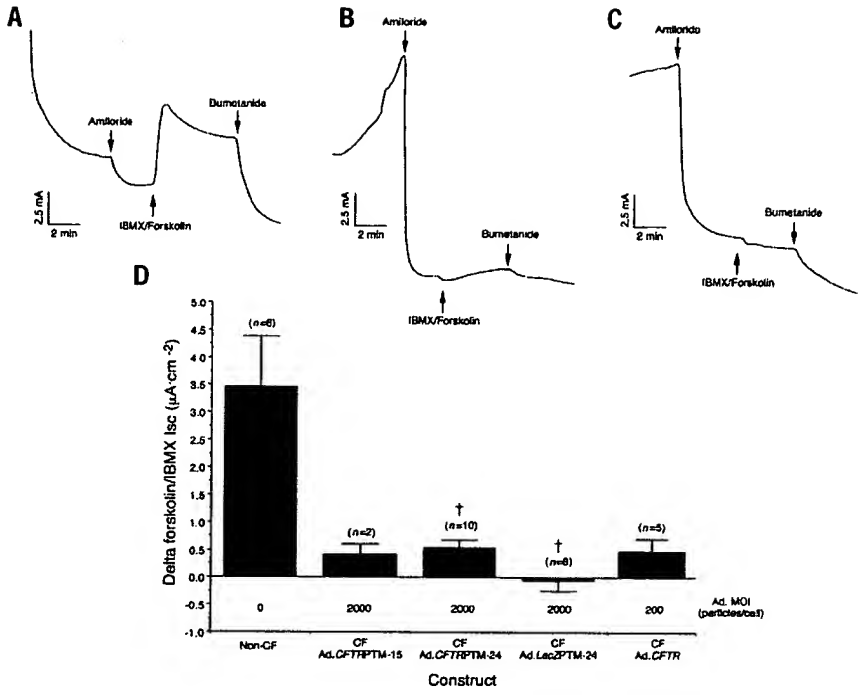

Figure 2. Transepithelial short-circuit currents in a ΔF508-homozygous CF model of polarized airway epithelia. Functional correction of CFTR-mediated chloride currents was evaluated in polarized CF epithelia following recombinant adenoviral expression of CFTR PTMs. (A–C) Typical short-circuit current (Isc) profiles under the various experimental conditions. After addition of amiloride (100 μM) to inhibit epithelial sodium conductance, IBMX (100μM)/forskolin (10 μM) was used to stimulate CFTR-mediated transepithelial Cl^- current. The maximum amplitude (μA) of the IBMX/forskolin response correlates with the magnitude of Cl^- transport across the epithelia and was used to calculate Isc_{max}. The sequential addition of bumetanide (100 μM) at the end of the experiment blocks all Cl^- movement into the cell from the basolateral membrane and serves as control for active transepithelial Cl^- transport under secretory conditions. The following Isc profiles are represented: (A) Non-CF airway epithelial culture; (B) Ad.*CFTR*PTM-24-infected ΔF508/ΔF508 CF epithelial culture; (C) Ad.LacZPTM-24-infected ΔF508/ΔF508 CF epithelial culture. (D) Graphical summary of the cumulative Isc data from multiple experiments. Results indicate the maximal mean (± s.e.m.) change in forskolin/IBMX-inducible Isc for *n* experiments. † Denotes statistically significant differences between values ($P < 0.01$) using the Student's *t*-test.

greater ($P < 0.001$) in Ad.*CFTR*PTM-24 (5.8 ± 0.6 mV) compared with Ad.*LacZ*PTM-24 (1.6 ± 0.7 mV) -infected CF xenografts. This change is indicative of increased Cl^- permeability and is consistent with the activation of CFTR Cl^- channels. In comparison with non-CF xenografts, which demonstrate an average ΔPD of −18.9 ± 3.2 mV under identical Cl^- secretory conditions[13], this 4.2 mV difference seen between Ad.*CFTR*PTM-24 and Ad.*LacZ*PTM-24 represents ~22% correction of normal CFTR function in the airway. This finding in xenografts is strikingly similar to the results obtained in polarized airway epithelia, where Ad.*CFTR*PTM-24 corrected Cl^- secretory Isc to a level 16% of that of non-CF samples. In summary, these studies demonstrated reasonably efficient correction of CFTR function in CF bronchial xenografts by SMaRT.

Discussion

Recent advances in RNA *trans*-splicing provide a spliceosome-mediated strategy for correcting gene defects at the RNA level[8,9]. One advantage of SMaRT is that only those cells expressing the targeted gene product can be corrected, avoiding potential problems associated with ectopic expression of a transgene. Given the heterogeneity of CFTR expression in the lung and complexities associated with its function, it has been theorized that reconstitution of endogenous CFTR expression may be required to restore normal electrolyte and fluid balance to the CF lung[3]. Furthermore, overexpression of CFTR in some cell lines has been found to decrease membrane potential and intracellular pH (ref. 15). Other studies have suggested that hyperexpression of CFTR causes expansion in cell volume and subsequent cell abnormalities[16] in addition to alteration of the physiological properties of the CFTR channel[17]. These observations suggest that overexpression of CFTR may be deleterious to airway cells. SMaRT provides one approach to circumvent these potential problems associated with high-level ectopic CFTR expression.

In this study we have demonstrated that SMaRT can restore partial function to endogenous ΔF508 CFTR. Correction has been confirmed by the detection of repaired mRNA, mature CFTR protein, and functional restoration of chloride transport. Furthermore, we provide functional evidence for SMaRT-mediated repair of endogenous pre-mRNA in two differentiated native CF airway epithelial models. Although quantification of *trans*-spliced CFTR protein in differentiated airway models was not possible because of insufficient material,

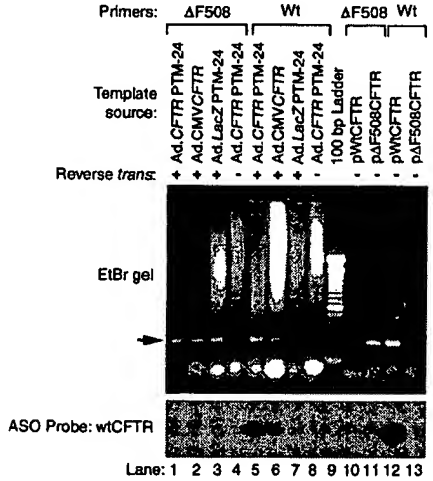

Figure 3. Evaluation of RNA *trans*-splicing repair by allele-specific RT-PCR and allele-specific oligonucleotide hybridization. Allele-specific primers were used to specifically amplify mutant ΔF508 (lanes 1–4) or wild-type F508 (lanes 5–8) mRNA from polarized epithelial cultures infected with adenoviral constructs. MOIs used for adenoviral infection were identical to that shown in Figure 2. PCR products were visualized on an ethidium bromide (EtBr) agarose gel (top panel). The omission of reverse transcriptase was used as a control for mRNA but not DNA amplification. Allele-specific plasmid controls containing either a mutant ΔF508 (lanes 11,13) or wild-type (lanes 10,12) CFTR cDNAs were used to confirm the specificity of the PCR reaction. Lane 9 contains a 100-bp DNA ladder. The arrow to the left of the gel indicates the appropriately sized CFTR amplification product. PCR products were evaluated by Southern blotting for the presence of the wild-type F508 codon using allele-specific oligonucleotide hybridization against a ^{32}P-labeled wtCFTR-specific antisense oligonucleotide probe (bottom panel).

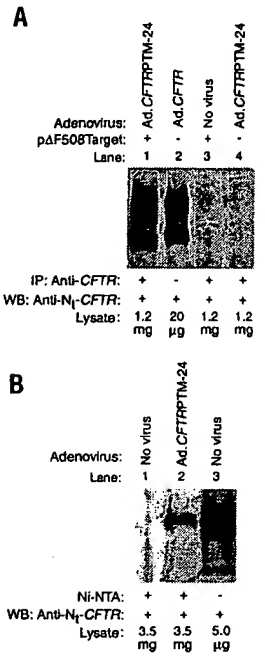

Figure 4. Immunodetection of *trans*-spliced CFTR protein. HeLa and T84 cells were evaluated for the ability of Ad.*CFTR*PTM-24 to produce fully processed CFTR protein from exogenous or endogenous pre-mRNA targets. (A) HeLa cells were transfected with a *CFTR* mini-gene target (pΔF508Target) expressing ΔF508 mRNA, followed by infection with Ad.*CFTR*PTM-24 (MOI 5,000 particles/cell). Controls included HeLa cells transfected with the mini-gene target or infected with Ad.*CFTR*PTM-24 alone. Following transfection and/or infection, cell lysates were immunoprecipitated with a rabbit anti-CFTR antibody, and western blots were performed with an N-terminal anti-CFTR antibody. As a positive control, Ad.CMV*CFTR* infection (MOI 5,000 particles/cell) was used. (B) T84 cells were used to evaluate the ability of Ad.*CFTR*PTM-24 to target endogenously produced CFTR mRNA. Ni-NTA magnetic agarose beads were used to capture *trans*-spliced full-length CFTR protein that contained a C-terminal His-tag. Both uninfected (lane 1) and Ad.*CFTR*PTM-24-infected (lane 2) T84 cells were evaluated. Following Ni-NTA precipitation, the level of immunoreactive CFTR proteins was evaluated by western blotting using an N-terminal anti-CFTR antibody. As a positive control, 5.0 µg of soluble membrane proteins from T84 cells were used (lane 3).

evidence in HeLa and T84 cells suggests a fairly low level of *trans*-spliced protein (0.2–2%). This is ~10-fold less efficient than the functional correction of chloride transport in polarized airway models (16–22%). Several factors may have influenced this finding. First, the efficiency of *trans*-splicing may be higher in polarized airway epithelia than in transformed cell lines. Second, the complementation profile necessary to achieve wild-type levels of CFTR chloride transport may be different from that for CFTR protein expression. We feel the latter rationale is the most plausible.

The quantity of CFTR mRNA necessary to retain a normal phenotype has been studied in a number of model systems. The most direct measurements were performed in phenotypically normal individuals with splicing polymorphisms that deleted part of nucleotide binding domain-1 (NBD1) from CFTR mRNA, leading to nonfunctional transcripts. These studies of phenotypically normal individuals with CFTR splicing polymorphisms suggest that only 8% of normal CFTR message is required for normal lung function[18]. Quantitative analysis has demonstrated that CFTR transcripts are expressed in nasal, tracheal, and bronchial epithelia at ~1–2 copies per cell in normal individuals[19]. Together, these studies provide an important conceptual framework for interpreting the efficiency of SMaRT in correcting CFTR-associated Cl^- transport abnormalities. An alternative interpretation of complementation arises from studies employing viral vectors expressing full-length CFTR cDNAs in airway models. In contrast to studies correlating phenotypes with the level of endogenous CFTR mRNA, gene transfer studies have determined the percentage of CFTR-overexpressing cells that is required to achieve functional correction. These studies have suggested that as little as 6% complementation is required to fully correct CFTR functional defects in Cl^- transport[20]. However, the setting in which a minority of cells express high levels of CFTR protein is probably quite different from the present study, where we presumed that the majority of airway cells express a small amount of CFTR protein at endogenous sites. The ability of an epithelium to properly regulate transepithelial Cl^- transport in the setting of high-level CFTR expression in a minority of cells stems from the potential of polarized airway epithelia to passively equilibrate Cl^- throughout the epithelial layer through cell–cell coupling[20]. We consider that the partial functional correction produced by SMaRT CFTR gene therapy is most analogous to that seen in phenotypically normal individuals with CFTR splicing polymorphisms who express low levels of CFTR protein in most of their airway cells.

Another explanation for the relatively high efficiency of *trans*-splicing to correct Cl^- transport abnormalities, in association with low protein expression, may stem from the fact that native CFTR protein expression in the airway is highly regulated[21,22]. Certain cell types in the airway express high levels of CFTR protein, while others, such as ciliated cells, have strikingly low concentrations of CFTR protein and mRNA but detectable levels of CFTR chloride channel activity[23,24]. The significance of this regulation is presently unclear, but it has been postulated to play a role in controlling ion flow across the epithelium[3]. In addition to transporting chloride, CFTR also regulates other channels such as epithelial sodium channel (ENaC). The coordinated activation of these channels is important in maintaining proper salt movement across the airway epithelium. Superimposed on this regulation is the fact that ENaC and other ion channels may have overlapping but distinct expression profiles in airway epithelial cells[3]. Thus, reconstitution of CFTR protein expression in the airway (even partial restoration) may be more efficient at complementing Cl^- transport defects than treatments generating supraphysiological expression of CFTR in the wrong cells. It is also important to recognize that Cl^- transport is only one index of CFTR function. Currently, it is unclear whether correction of bulk Cl^- transport across the airway epithelium alone will prevent or reverse lung disease in CF. If indeed Cl^- transport is the only functional defect in CFTR responsible for lung disease, then SMaRT may not have the therapeutic potential conferred by cDNA vectors that express large quantities of CFTR in some airway cells. Resolution of this question awaits the development of authentic animal models for CF lung disease.

Several aspects of the present study are worth noting when interpret-

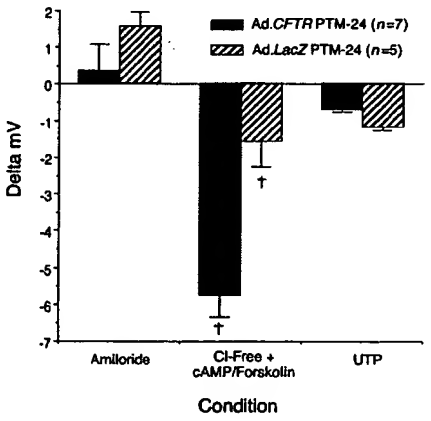

Figure 5. *In vivo* complementation of CFTR Cl^- permeability defects in ΔF508/ΔF508 CF bronchial xenografts. To evaluate the ability of *trans*-splicing to functionally correct CFTR defects in a human CF airway model, ΔF508/ΔF508 CF xenografts were infected with either Ad.*CFTR*PTM-24 or Ad.LacZPTM-24, and potential difference measurements were evaluated under conditions that stimulate CFTR activity. Data represents the mean (±s.e.m.) change in mV responses to amiloride, cAMP/forskolin, and UTP for *n* independent xenografts. † Denotes statistically significant differences between values ($P < 0.001$) using the Student's *t*-test.

ing the clinical utility of SMaRT technology for gene therapy of cystic fibrosis. First, the model systems and delivery vector (i.e., recombinant adenovirus) were chosen to test the feasibility of SMaRT for correcting endogenous CFTR defects and not the clinical application of this technology. For example, recombinant adenovirus in all likelihood will not be the vector of choice for gene therapy to the lung, because it is relatively ineffective at transducing airway epithelia from the apical surface. Although this vector system was effectively used to test SMaRT, the delivery methods used in the present study are not directly translatable to clinical *in vivo* use (i.e., basolateral infection or serial infection with vector at high titers). Recombinant adeno-associated virus (rAAV) will probably be the vector of choice for clinical applications in CF from an efficacy and safety standpoint. Second, the choice of vector system will also determine whether the therapeutic application of SMaRT will provide long-term correction. Integrating SMaRT vectors (i.e., rAAV) have the potential to provide long-term correction if stem cells in the airway are transduced, whereas nonintegrating vectors such as recombinant adenovirus can only provide transient correction. Finally, additional theoretical limitations of SMaRT that remain to be addressed include the potential of *trans*-splicing into non-CFTR mRNAs.

Our findings demonstrate the potential feasibility of applying SMaRT technology to the gene therapy of cystic fibrosis. Genetic reprogramming of RNA by SMaRT may also have utility for many other disorders. SMaRT technology fills a specific niche in gene therapy that allows for native expression of corrected gene products without the need for complex regulatory elements capable of delivering gene products at their endogenous sites of expression. This will have the greatest utility for diseases in which ectopic expression of a gene product has deleterious consequences or when a mutated gene product gives rise to a dominant negative phenotype. Furthermore, as PTM expression cassettes can be much smaller than those encoding full-length cDNAs, SMaRT also allows for the use of smaller vectors such as rAAV with limited packaging capacity. In the case of CFTR delivery this is particularly relevant as the full-length CFTR cDNA can just fit into a rAAV vector, leaving no space for a promoter.

Experimental protocol

Generation of recombinant adenoviruses expressing *trans*-splicing PTMs. The structure of PTMs targeting intron 9 of CFTR have been described[8]. The structure of PTM-24 and PTM-15, and the proposed *trans*-splicing mechanism between the PTM and CFTR pre-mRNA, are illustrated in Figure 1. These PTMs were incorporated into recombinant adenoviruses (Ad.*CFTR*PTM-15 and Ad.*CFTR*PTM-24) and are designed to replace CFTR exons 10–24. Plasmids containing CFTR PTM-24 or CFTR PTM-15 were digested with *Nhe*I and *Pme*I, blunt-ended, and subcloned into the pAd.CMV-link plasmid[25] at the *Eco*RV site. Recombinant adenovirus was generated from these proviral plasmids (pAd.*CFTR*PTM-15 and pAd.*CFTR*PTM-24) as described[26]. Similarly, two control adenoviral vectors (Ad.LacZPTM-15 and Ad.LacZPTM-24), with a LacZ 3′-exon, were also generated[12]. The particle:plaque-forming unit ratio (particle:PFU) was typically equal to 25 for all constructs.

Short-circuit current (Isc) measurement in polarized airway epithelia. Freshly isolated human airway epithelial cells from either non-CF or ΔF508-homozygous CF bronchial airways were seeded in 12-mm Millicell culture inserts (Millipore, Bedford, MA) pre-coated with collagen. Methods for generating these air/liquid interface cultures were as described[27]. A transepithelial resistance of >500 indicated the proper formation of tight junctions and the readiness of a monolayer for Isc measurement. The airway cultures were infected with 50 µl of virus-containing medium to the basolateral side of the epithelia at an MOI of 200–2,000 particles/cell. The cells were incubated at 37°C for 2 h before the epithelia were returned to 0.6 ml of basolateral medium and incubated for an additional 48 h. Gene transfer efficiency was evaluated using an Ad.GFP vector and demonstrated transduction of >90% airway cells at an MOI of 2,000 particles/cell. Transepithelial short-circuit currents were measured using an epithelial voltage clamp and a self-contained Ussing chamber as described[28]. Throughout the experiment, the chamber was maintained at 37°C and aerated with O_2. The basolateral side of the chamber was filled with buffered Ringer's solution containing 135 mM NaCl, 1.2 mM $CaCl_2$, 1.2 mM $MgCl_2$, 2.4 mM KH_2PO_4, 0.2 mM K_2HPO_4, and 5 mM HEPES, pH 7.4. The apical side of the chamber was filled with a low-chloride Ringer's containing 135 mM sodium gluconate, 1.2 mM $CaCl_2$, 1.2 mM $MgCl_2$, 2.4 mM KH_2PO_4, 0.2 mM K_2HPO_4, and 5 mM HEPES, pH 7.4. Transepithelial voltage was clamped at zero, and the resulting Isc was measured and recorded. Voltage was referenced to the apical compartment. The series resistance of the Ringer's solution and transwell membrane was electrically compensated before initiating experiments. All chemical agonists and antagonists were added to both the apical and the basolateral sides of the monolayer by direct injection and mixed by aerating the Ringer's.

Detection of repaired CFTR mRNA by RT-PCR and Southern blotting. Polarized airway epithelial cultures prepared from non-CF or ΔF508-homozygous human bronchial epithelial cells were infected with recombinant adenovirus as described above. Cells were harvested into lysis buffer (Qiagen Total RNA Isolation kit; Qiagen, Valencia, CA) at 48 h post infection and pooled for each group composed of four identical cultures. Total RNA was isolated using a Qiagen Total RNA Isolation kit, cDNA was synthesized using a RT-PCR kit from Invitrogen (Carlsbad, CA), and the repaired CFTR mRNA was amplified by two rounds of PCR using the following primers:

Primer A: 5′-AGAATGTAACAGCCTTCTGGGAGG-3′
Primer B: 5′-AGAAATTCTTGCTGGTTGACCTCC-3′
Primer C: 5′-CTTCTTGGTACTCCTGTCCTG-3′
Primer D: 5′-ATCATAGGAAACACCAAAGATGA-3′
Primer E: 5′-TCATAGGAAACACCAATGATAT-3′.

The outer primers (primers A and B) were designed to amplify a 500-bp region harboring the F508 region. The inner primers were composed of a common forward primer (primer C) for both the *cis*- and *trans*-spliced products, but different reverse primers based on either the wild-type F508 (primer D) or ΔF508 sequences (primer E). The PCR products were resolved by electrophoresis, and Southern blot hybridization was performed with a ^{32}P-labeled allele-specific oligonucleotide for the wild-type F508 sequence (5′-CATCTTTGGTGTTTCCT-3′).

Detection of repaired CFTR protein by immunoblotting. HeLa cells were transfected with a *CFTR* mini-gene target construct[8] using Lipofectamine (Life Technologies, Gaithersburg, MD). After transfection, the cells were infected with Ad.*CFTR*PTM-24 (MOI of 5,000 particles/cell) for 48 h and harvested by the addition of lysis buffer (20 mM Tris, 2% CHAPS, 150 mM NaCl, pH 7.4, containing a protease inhibitor cocktail tablet) and cleared by centrifugation. The supernatants were then immunoprecipitated with anti-CFTR polyclonal antibody (Santa Cruz Biotechnology, Inc., Santa Cruz, CA) followed by western blotting with an N-terminal anti-CFTR monoclonal antibody (Upstate Biotechnology Inc., Lake Placid, NY). Immunoreactivity was detected with peroxidase-conjugated secondary antibody using an ECL detection kit.

The production of reprogrammed CFTR protein from endogenous mRNA was evaluated using T84 cells. T84 cells were infected with Ad.*CFTR*PTM-24 (MOI of 5,000 particles/cell) and harvested at 48 h post infection. Cells were lysed by passing five times through a 25-gauge needle. Lysates were then centrifuged at 1,500 *g* for 10 min at 4°C to remove large particulate material and centrifuged again at 100,000 *g* for 1 h at 4°C to isolate the pelleted membrane fraction. Membrane pellets were resuspended with lysis buffer and incubated for 30 min at 4°C and centrifuged at 100,000 *g* for 1 h at 4°C. The supernatant containing the soluble membrane proteins were used for immunoprecipitation and western blotting. Briefly, His-tagged CFTR in the supernatant was affinity-purified using Ni-NTA Magnetic Agarose Beads (Qiagen). Western blotting was done with an anti-N-terminal CFTR antibody following the same procedure described above.

PTM-mediated repair of ΔF508 CFTR in human bronchial xenografts. Human bronchial xenografts were generated from primary ΔF508 homozygous CF bronchial airway epithelial cells as described[27]. Xenografts were sequentially infected *in vivo* twice at 16-h intervals with 1×10^{12} particles of Ad.*CFTR*PTM-24 starting at five to six weeks post-transplantation. This level of infection provides ~50% transduction, as evidenced by recombinant adenoviral reporter gene expression[14]. Xenografts were analyzed 72 h after the last infection by monitoring cAMP-induced changes in transepithelial PD as described[13]. The cAMP-induced Cl^- permeability was continuously